Materials Science in Semiconductor Processing 174 (2024) 108220

Contents lists available at ScienceDirect

Materials Science in Semiconductor Processing

journal homepage: www.elsevier.com/locate/mssp

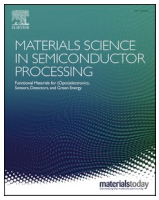

Integration of graphene and MoS_2 on silicon carbide: Materials science challenges and novel devices

Filippo Giannazzo [a,*], Salvatore Ethan Panasci [a], Emanuela Schilirò [a], Antal Koos [b], Béla Pécz [b]

[a] Consiglio Nazionale Delle Ricerche - Istituto per La Microelettronica e Microsistemi (CNR-IMM), Strada VIII 5, 95121, Catania, Italy
[b] HUN-REN Centre for Energy Research, Institute of Technical Physics and Materials Science, Konkoly-Thege Ut 29-33, 1121, Budapest, Hungary

ARTICLE INFO

Keywords:
Graphene
MoS_2
Silicon carbide
Heterogeneous integration
Electronic devices
Sensors

ABSTRACT

Although silicon carbide (SiC) is widely regarded as the material of choice for power electronics, the development of several new applications on the SiC material platform is currently explored. The integration of two dimensional (2D) materials, such as graphene and molybdenum disulfide (MoS_2) provides silicon carbide (SiC) with additional functionalities, allowing to expand its range of applications. This article reviews the state-of-the art methods for scalable growth of graphene and MoS_2 on SiC, specifically on the hexagonal polytypes. Some open research directions in materials integration have been also discussed, like the use of epitaxial graphene (Epi-Gr) as interlayer for van der Waals (vdW) epitaxy of GaN or Ga_2O_3 on SiC substrates, and the growth of 2D forms of GaN materials by confined epitaxy at Epi-Gr/SiC interface. Finally, an overview of recently proposed electronics/optoelectronics applications of these material systems, specifically for high frequency electronics, quantum metrology, THz and UV detectors, is provided. This work can be a useful guide for silicon carbide community on these open research directions.

1. Introduction

Two-dimensional (2D) layered materials are the class of materials composed by stacks of 2D crystalline sheets bond by van der Waals (vdW) interaction. These materials have been the object of intensive investigations during last 20 years, starting from early reports on graphene exfoliation from HOPG by Geim and Novoselov [1] and the nearly contemporary studies on the graphenization of silicon carbide (SiC) surface by de Heer [2]. Nowadays, hundreds of 2D materials have been investigated experimentally [3], whereas a database of up to 6000 monolayer structures has been recently compiled by predictive computational studies [4]. Noteworthy, the 2D materials family covers the entire range of electronic transport properties, including semimetals (such as graphene), semiconductors (such as transition metal dichalcogenides [5] and phosporene [6]) and insulators (h-BN) [7]. This offered the possibility of realizing electronic/optoelectronic devices and sensors entirely composed by 2D materials [8,9], although the used fabrication approaches (i.e. the sequential exfoliation and stacking of different 2D sheets) are clearly suitable only for research purposes. Alternatively, the integration of 2D materials with conventional bulk semiconductors (such as Si, Ge, SiC and GaN) has been also widely explored, with the aim to enhance the performances of state-of-the-art electronic/optoelectronic devices and sensors [10–17].

In this context, silicon carbide (SiC) represents a very interesting case. Due to the intrinsic material properties (wide bandgap, high critical electric field, and high thermal conductivity) [18] and following the huge improvement in 4H-SiC wafers size and quality during last 20 years, SiC became a key enabling technology for high-power devices, with pervasive applications in energy conversion systems, automotive, and aerospace [19]. Recently, emerging applications of SiC beyond power electronics have attracted an increasing interest [20]. As an example, some research groups are actively working to develop SiC-based complementary-metal-oxide-semiconductor (CMOS) devices and integrated circuits to be employed under extreme conditions (high temperature, radiation and space environments), which are incompatible with conventional Si CMOS technology. Due to its unique photonic properties (wide optical transmission window from near UV to mid-infrared, high second-order nonlinear susceptibility, rather high refractive index), SiC is also currently considered for photonics and quantum photonic integrated circuits [21,22]. Its excellent mechanical properties make SiC a material of choice for micro- and nano-electro-mechanical-systems (MEMS and NEMS) [23,24]. Finally,

* Corresponding author.
E-mail address: filippo.giannazzo@imm.cnr.it (F. Giannazzo).

https://doi.org/10.1016/j.mssp.2024.108220
Received 23 December 2023; Received in revised form 5 February 2024; Accepted 6 February 2024
Available online 10 February 2024

due to its high biocompatibility, SiC has been employed for biosensors and "in vivo" biomedical applications [25].

The integration of 2D materials on SiC provides it with additional functionalities, and allows to expand its spectrum of applications [26]. As an example, the growth of high electron mobility epitaxial graphene (Epi-Gr) on semi-insulating SiC wafers allowed to demonstrate radio frequency (RF) transistors with hundreds GHz cut-off frequency and integrated circuits [27,28]. Furthermore, the excellent electronic properties of the Epi-Gr two-dimensional electron gas (2DEG) have been exploited in quantum metrology, with the demonstration of a quantum Hall effect resistance standard [29] overcoming some of the limitations of the conventional standard based on the AlGaAs/GaAs 2DEG [30]. The combination of the excellent conductivity and optical transmittance of graphene (~97.7% from near IR to UV for a monolayer) makes it an optimal transparent conductive electrode for optoelectronic applications of SiC, such as UV photodetectors [31]. Due to its high surface-to-volume ratio, the transport properties of Epi-Gr are highly sensitive to the interaction with surrounding environment, enabling the realization of gas or chemical sensors with excellent sensitivity [32,33], although optimizing selectivity still remains a challenge. Proper surface functionalization strategies of Epi-Gr also allowed to demonstrate biosensors targeted for the point-of-care and label-free diagnostics of several kind of diseases [34,35]. Besides Epi-Gr, the deposition of 2D semiconductors, such as molybdenum disulfide (MoS_2), on the surface of SiC has been investigated in the last years using different methods [36–41], and the obtained MoS_2/SiC semiconductor heterostructures have been considered for applications like heterojunction diodes [36,37,41], dual band (visible/UV) photodetectors [39], and in (photo)electro-catalytic hydrogen evolution reactions [40].

This review article provides an overview on the state-of-the art of graphene and MoS_2 integration on SiC (specifically on the hexagonal polytypes), and illustrates recently proposed electronics/optoelectronics applications of these material systems, specifically for high frequency electronics, quantum metrology, THz and UV detectors. Some open research directions in materials integration were also discussed, like the use of Epi-Gr as interlayer for van der Waals epitaxy of GaN on SiC, and the growth of 2D forms of GaN materials by confined epitaxy at Epi-Gr/SiC interface.

2. 2D materials growth on silicon carbide: state of the art

2.1. Epitaxial graphene (Epi-Gr) by high temperature decomposition of SiC

High temperature annealing processes, resulting in the controlled graphitization of SiC surface, represented one of the first methods to obtain graphene directly on a semiconductor or semi-insulating substrate, i.e. ready for electronic devices fabrication [2,42,43]. Upon high temperature annealing, preferential Si sublimation from SiC surface leaves an excess of carbon (C) atoms, which migrate and reorganize in the 2D hexagonal graphene lattice. So far, this method has been widely employed to obtain Epi-Gr on the hexagonal 4H and 6H polytypes of SiC. The growth on the cubic (3C) polytype has been also investigated [44,45], since it offers the possibility of integrating graphene with 3C-SiC layers on large-area and low-cost silicon wafers. However, the material quality of heteroepitaxial 3C-SiC, typically characterized by the presence of a high density of conducting defects [46], need to be further optimized in order to exploit graphene grown on its surface in electronic applications.

The structural and electronic properties of Epi-Gr grown on hexagonal (6H and 4H) SiC substrates are strongly dependent on the graphitization conditions (i.e. temperature and pressure in the furnace chamber) and on the crystal orientations [47], with very different results obtained on the Si face (0001) [48], the C face (000–1) [49], and the non-polar faces (11–20) and (1–100) [50,51].

As shown in Fig. 1(a–b), under ultra-high-vacuum (UHV) conditions,

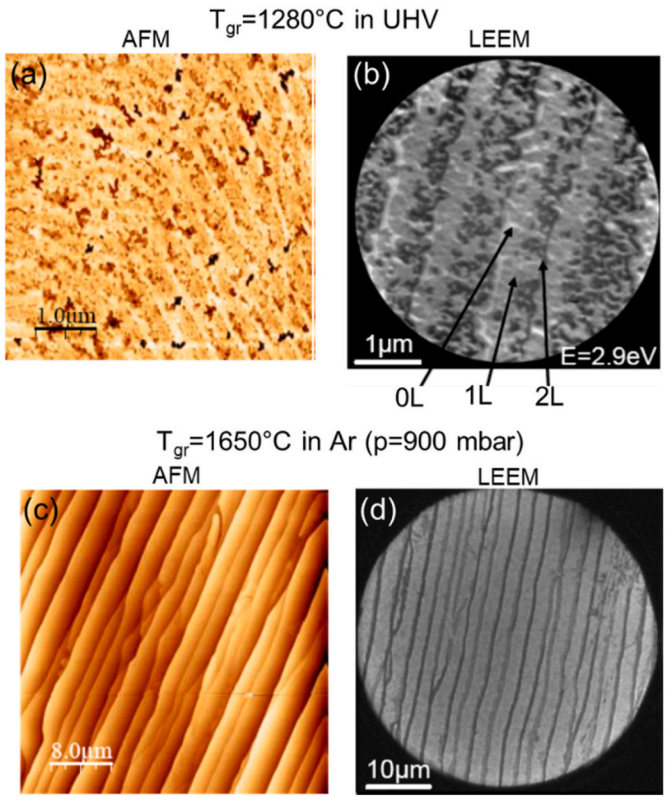

Fig. 1. (a) Atomic force microscopy (AFM) morphology and (b) low energy electron microscopy (LEEM) images of Epi-Gr on 6H-SiC(0001) formed by annealing in UHV at a temperature T_{gr} = 1280 °C. The light, medium and dark grey contrast in the LEEM image correspond to a local thickness of 0L, 1L and 2L, respectively. (c) AFM morphology and (d) LEEM image of Epi-Gr on 6H-SiC (0001) formed by annealing in Ar (p = 900 mbar, T_{gr} = 1650 °C). SiC terraces are uniformly covered by 1L Epi-Gr, whereas 2L/3L Epi-Gr are present at step edges. Images adapted with permission from Ref. [42].

Epi-Gr formation on the surface of on-axis SiC(0001) has been obtained even at relatively low temperatures (T_{gr} = 1280 °C), but the low surface mobility of C adatoms gave rise to a very inhomogeneous graphene coverage. On the other hand, annealing of on-axis SiC(0001) at higher temperature (T_{gr} = 1650 °C) under inert gas (Ar) at atmospheric pressure (p = 900 mbar) resulted in a highly-uniform monolayer (1L) epitaxial graphene coverage, with a small density of bilayer (2L) or trilayer (3L) patches present at SiC step edges (see Fig. 1(c) and (d)). Instead, in the case of 8° or 4° off-axis SiC(0001) samples, Bernal stacked graphene multilayers epitaxially aligned with the substrate are typically obtained [52–54]. Conversely, graphene growth on the (000–1)face and non-polar faces occurs in a less controlled way, yielding a laterally inhomogeneous distribution of reciprocally misaligned multilayers, without epitaxial relation with the substrate [55,56].

It is worth mentioning that, although thermal decomposition in Ar gas ambient is the most widely used approach for Epi-Gr growth on SiC surface, some research groups adopted high temperature chemical vapor deposition (CVD) with propane (mixed to Ar or H_2) as hydrocarbon gas precursor [57–59]. Clearly, this additional carbon supply in the growth process provides wider flexibility in the Epi-Gr formation conditions.

The excellent uniformity of Epi-Gr on SiC(0001) originates from the peculiar growth mechanism, initiated by the formation of a $(6\sqrt{3} \times 6\sqrt{3})R30°$ surface reconstruction, commonly named buffer layer (BL) or "zero layer", which consists of a partially sp^3 hybridized C layer due to covalent bonds to the Si face (see Fig. 2(a), (c)) [60]. Monolayer graphene is subsequently generated by further sublimation of SiC underneath, resulting in the formation of a new buffer layer and the conversion of the previous one in a sp^2 carbon sheet (see Fig. 2(b), (d)).

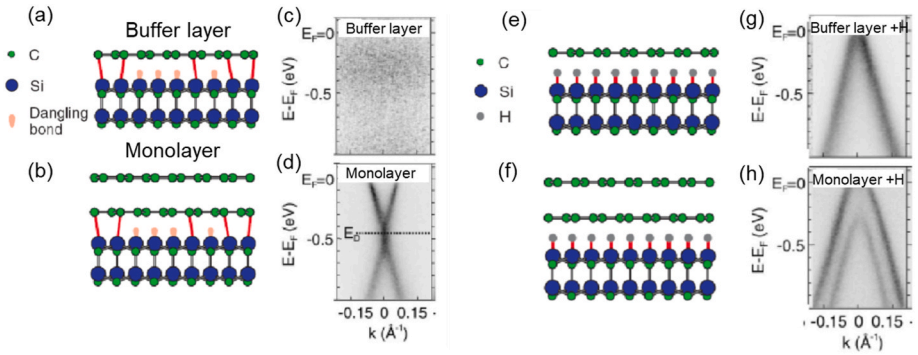

Fig. 2. Schematic illustration of the interface structure for the C buffer layer (a) and Epi-Gr monolayer (b). The corresponding energy-wavenumber E-k dispersions, measured by angle resolved photoemission spectroscopy (ARPES) are reported in (c) and (d). Illustration of the QFSMG (e) and QFSBG (f) obtained after hydrogen intercalation of the buffer-layer and monolayer Epi-Gr, respectively. The corresponding ARPES analyses are reported in (g) and (h). Images adapted with permission from Ref. [63].

One of the most interesting features of the Epi-Gr/SiC system is the possibility of tuning both the electronic properties of graphene and its heterointerface with SiC by intercalation of different types of atomic species [61,62]. As an example, hydrogen intercalation has been shown to be effective in the breaking of covalent bonds between the BL and SiC (0001) and the saturation of Si dangling bonds, thus transforming the BL (Fig, 2a),(c)) into a quasi-free-standing monolayer graphene (QFSMG) (Fig. 2(e),(g)), and a monolayer Epi-Gr (Fig. 2(b),(d)) into a quasi-free-standing bilayer graphene (QFSBG) (Fig. 2(f),(h)) [63,64].

The BL between Epi-Gr and the Si face of SiC is responsible of a high n-type doping (10^{13} cm^{-2}) of Epi-Gr (induced by the high density of positively charged Si dangling bonds) and of the relatively low electron mobility, in the range from ~2000 to ~1000 $cm^2V^{-1}s^{-1}$ (as illustrated in Fig. 3(a)). On the other hand, the quasi-free-standing Epi-Gr typically exhibits a mild p-type doping (~5×10^{12} cm^{-2}), due to the polarization effect from the SiC substrate, and an enhanced carrier mobility (>3000 $cm^2V^{-1}s^{-1}$) nearly independent on the temperature. Furthermore, from the view-point of vertical current injection at graphene/SiC interface, as grown monolayer Epi-Gr (with the interfacial BL) exhibits an Ohmic contact behavior even on lowly n-type doped SiC (N_D-$N_A \approx 10^{16}$ cm^{-3}), as illustrated in Fig. 3(c),(d). Instead, a rectifying behavior (with a Schottky barrier height $\Phi_B \approx 0.9$ eV) has been obtained from the same Epi-Gr/SiC(0001) heterojunctions after H intercalation [65,66], as shown on Fig. 3(e), (f). The properties of this Schottky barrier have been investigated in detail, also by nanoscale resolution electrical analyses (conductive AFM), showing the presence of inhomogeneities mainly associated to the SiC substrate steps [67]. Furthermore, the correlation between the homogeneity of hydrogen intercalation and the uniformity of the Schottky barrier has been investigated by combining Raman mapping and local current-voltage analyses by C-AFM [68].

By exploiting the possibility of locally engineering the current transport at Epi-Gr/SiC interface by selective area H_2 intercalation, Hertel et al. [66,69] demonstrated a monolithic graphene/SiC transistor structure, where the channel is formed by n-type (~10^{15} cm^{-3}) epitaxial 6H-SiC on top of p^+-SiC (~2×10^{18} cm^{-3}), and with the source/drain Ohmic contacts and the gate Schottky contact made with Epi-Gr (see schematics in Fig. 4(a)). The current transport in the SiC channel was modulated both by the backgate bias V_{BG} (which controlled the space charge region of the p^+/n SiC junction), and by the topgate bias (V_{TG}) applied to the Epi-Gr Schottky contact. Representative transfer and output characteristics of this device are reported in Fig. 4(b) and (c), respectively.

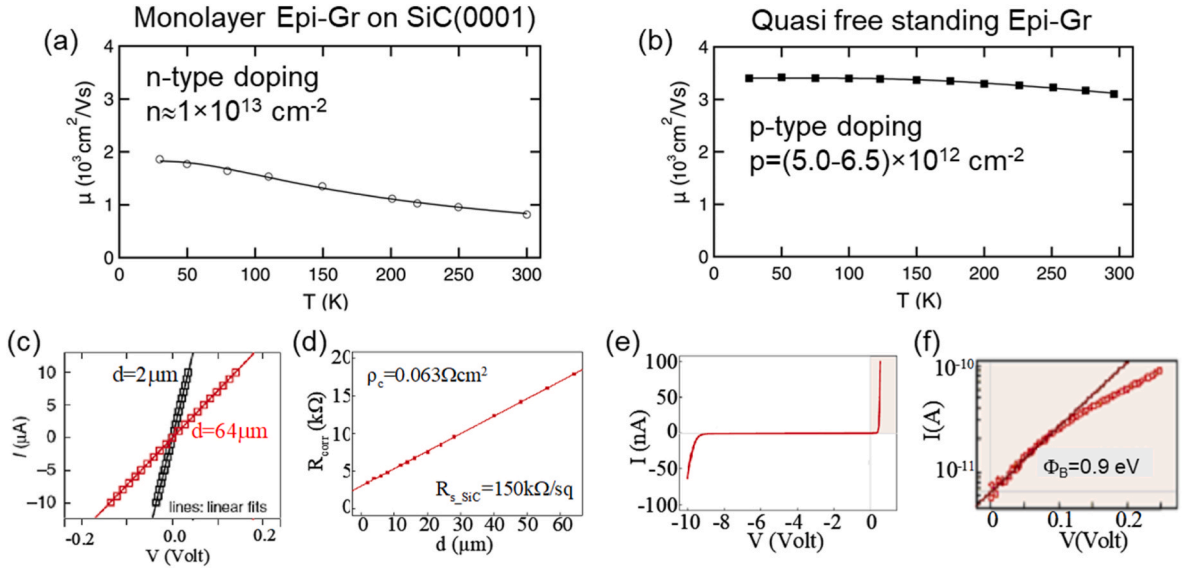

Fig. 3. Temperature dependence of the Hall effect mobility for (a) monolayer Epi-Gr grown on 6H-SiC(0001) and (b) QFSMG, obtained by H intercalation of the buffer layer. (c) Ohmic contact behavior of monolayer Epi-Gr/SiC(0001) interface, measured using circular TML test patterns, and (d) evaluation of the contact resistance. (e) Rectifying contact behavior of the QFSBG and (f) evaluation of the Schottky barrier height. Panels (a) and (b) adapted from Ref. [61]. Panels (c), (d), (e) and (f) adapted from Ref. [66].

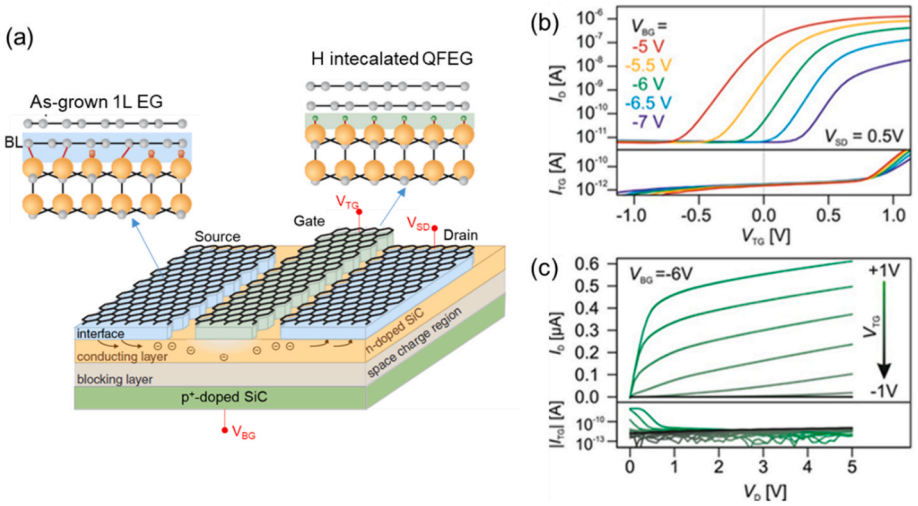

Fig. 4. (a) Schematic of a monolithic Epi-Gr/SiC transistor, with the source/drain Ohmic contact formed by as grown 1L Epi-Gr and the top-gate contact formed by QFSBG obtained by selective area H intercalation. Current transport in the n-SiC conducting channel is controlled both by the local top-gate bias (V_{TG}) and the global back-gate bias (V_{BG}) modulating the space charge region of the p^+-SiC/n-SiC junction- (b) Transfer characteristics I_D-V_{TG} and top gate leakage current (I_{TG}) for different values of the back-gate bias. (c) Output characteristics and top-gate leakage for fixed back-gate bias ($V_{BG} = -6V$) and different V_{TG} values. Panel (a) adapted with permission from Ref. [66]. Panels (b) and (c) adapted with permission from Ref. [69].

A very recent development in the field of epitaxial graphene on SiC has been the demonstration of semiconducting epi-graphene (SEG) with a band gap of 0.6 eV and room temperature carrier mobility μ>5000 $cm^2\ V^{-1}s^{-1}$ on the (0001) face of on-axis SiC [70]. The SEG has been obtained using a quasi-equilibrium annealing method at a temperature of 1600 °C, when the SiC(0001) face is placed in contact with a SiC (000–1) sample, and a small temperature gradient allows diffusion of carbon atoms from the (000–1) face to the (0001) face. This results in the formation of an ordered buffer layer on the SiC(0001) terraces, which exhibits the above mentioned semiconducting properties.

2.2. Molybdenum disulfide (MoS_2) on SiC by CVD and PLD

Besides the semi-metallic graphene, the integration of layered semiconductors, such as the 2H-MoS_2, on silicon carbide has been recently explored. A MoS_2 monolayer (1L) is formed by a plane of Mo atoms sandwiched between two planes of S atoms with covalent bonds, whereas MoS_2 multilayers are composed by the stacking of MoS_2 layers connected by weak vdW bonds. Noteworthy, MoS_2 exhibits a thickness dependent energy bandgap, i.e. E_g≈1.2–1.3 eV (indirect bandgap) for two/three layers to multilayers of MoS_2, which increases to E_g≈1.8–1.9 eV (direct bandgap) for 1L MoS_2 [71]. Furthermore, carrier mobility values up to ~200 $cm^2\ V^{-1}s^{-1}$ have been reported for 1L-MoS_2 [72]. These bandgap values make the combination of MoS_2 with the wide bandgap (WBG) 4H-SiC attractive for the fabrication of high responsivity photodetectors sensitive both to the visible and the UV spectral range [39]. Furthermore, the dangling-bonds-free nature of MoS_2 layers offers the possibility of realizing MoS_2/4H-SiC heterojunction diodes with atomically abrupt interfaces [36,37,41]. In this respect, the epitaxial growth of semiconducting 2H-MoS_2 on 4H-SiC is favored by the low basal plane lattice constants mismatch (~2.9%), as illustrated in the plot in Fig. 5. So far, different deposition approaches, including chemical vapor deposition (CVD) [38,39,73] and pulsed laser deposition (PLD) [41,74], have been explored for the direct growth of MoS_2 on SiC.

CVD growth of MoS_2 is typically performed within a quartz tube using vapors emitted from crucibles with S and MoO_3 powders, which are transported by an inert carrier gas (Ar) to the substrate, heated at a temperature of 700–800 °C. This approach typically results in the nucleation and growth of triangular shaped crystalline MoS_2 domains with lateral sizes ranging from hundreds of nanometers to several micrometers [73]. However, achieving uniform coverage on wafer scale

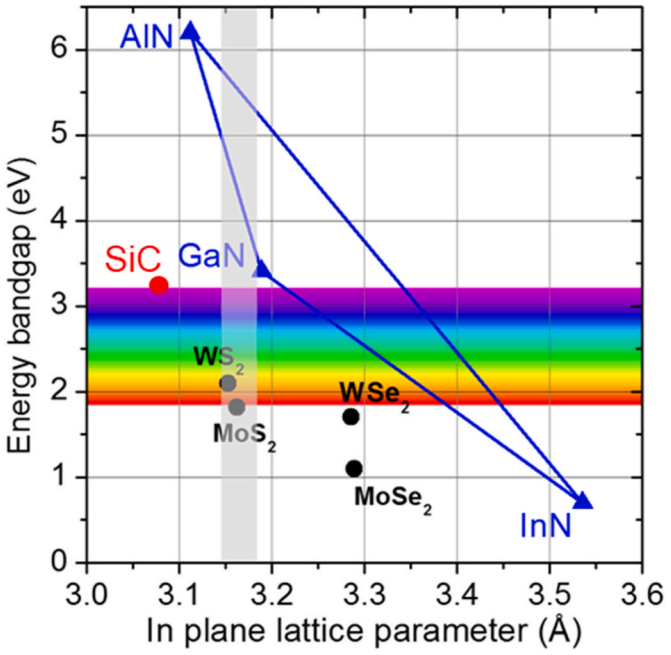

Fig. 5. Plot of the energy bangdap vs the in-plane lattice parameter for 4H-SiC, group-III Nitrides (GaN, AlN and InN), and common monolayer transition metal dichalcogenides (MoS_2, WS_2, $MoSe_2$, WSe_2).

represents a challenge, due to the difficulty of controlling the vapor flows for the two precursors, especially MoO_3, on the entire wafer area. Alternatively, the sulfurization of thin Mo or MoO_x films pre-deposited by physical vapor deposition (e.g. evaporation or sputtering) represents an effective method to obtain uniform MoS_2 coverage on large area and on different kind of substrates [75,76]. In this case, a good control of the MoS_2 film thickness has been achieved down to the monolayer level [37], by properly calibrating the initial Mo or MoO_x film thickness and the sulfurization temperature. This latter approach has been employed by different research groups to demonstrate p^+-MoS_2/n^+-4H-SiC heterojunction tunnel diodes for low power consumption and fast-switching applications. As an example, p^+-doped MoS_2 multilayers

on a n^+ 4H-SiC substrate have been obtained by Lee et al. [36] by high temperature (1000 °C) sulfurization of thin Mo/Nb/Mo stacks, where Nb atoms had the role of acceptors for MoS_2. Although degenerate p-type doping of MoS_2 was obtained, the current injection across these p^+ MoS_2/n^+ SiC heterojunctions was found to be dominated by midgap states in SiC, probably related to interface defects introduced by the high temperature process [36]. More recently, the sulfurization of very-thin (≈1.2 nm) Mo films on n^+ 4H-SiC at a temperature of 700 °C in a two heating zones tube furnace (see illustration in Fig. 6(a)) resulted in the formation of a highly uniform p^+-MoS_2/n^+-4H-SiC heterostructure [37]. The degenerate p^+-type doping of MoS_2 was explained by the presence of a significant amount of MoO_3 in the MoS_2 film, as demonstrated by XPS analyses. High resolution structural/chemical analyses by cross-sectional electron microscopy (Fig. 6(b),(c)) demonstrated the formation of 1L MoS_2 on the SiC surface. The monolayer uniformity on large area was also demonstrated by micro-Raman mapping. Finally, the current injection through MoS_2 heterojunctions with a n-type (~10^{16} cm^{-3}) 4H-SiC epitaxial layer and with a n^+-doped (~10^{19} cm^{-3}) 4H-SiC substrate was investigated by current-voltage (I-V) characteristics collected by a conductive AFM tip, as illustrated in Fig. 6(c) and (d). While the MoS_2/n-SiC junction showed a rectifying behavior, with very low current at negative bias and a current onset at a relatively high positive bias of 4 V, the MoS_2/n^+-4H-SiC junction featured an increased current under both polarizations, accompanied by a pronounced negative differential resistance (NDR) for positive bias. This latter was the first demonstration of band-to-band tunneling between degenerately p^+ doped 1L MoS_2 and n^+-doped SiC, confirming the abruptness of this 2D/3D van der Waals interface.

PLD from a MoS_2 target under high vacuum has been also employed to deposit ultra-thin MoS_2 films on large area with excellent thickness uniformity [74,77]. Recently, this method has been used to fabricate heterojunction diodes between n-type doped 3L MoS_2 and 4H-SiC(0001) samples with different doping levels, i.e. n^- epitaxial doping (~10^{16} cm^{-3}) and n^+ ion implantation doping (>10^{19} cm^{-3}) [41]. The SiC surface doping allowed a wide tunability of the current injection at the MoS_2/SiC interface, with a highly rectifying behavior in the case of MoS_2/n^- SiC junction, and a strongly enhanced reverse current for MoS_2/n^+ SiC one. Thermionic emission was the dominant mechanism ruling forward current in MoS_2/n^- SiC diodes, with an effective barrier Φ_B=(1.04 ± 0.09) eV and an ideality factor close to unity. Instead,

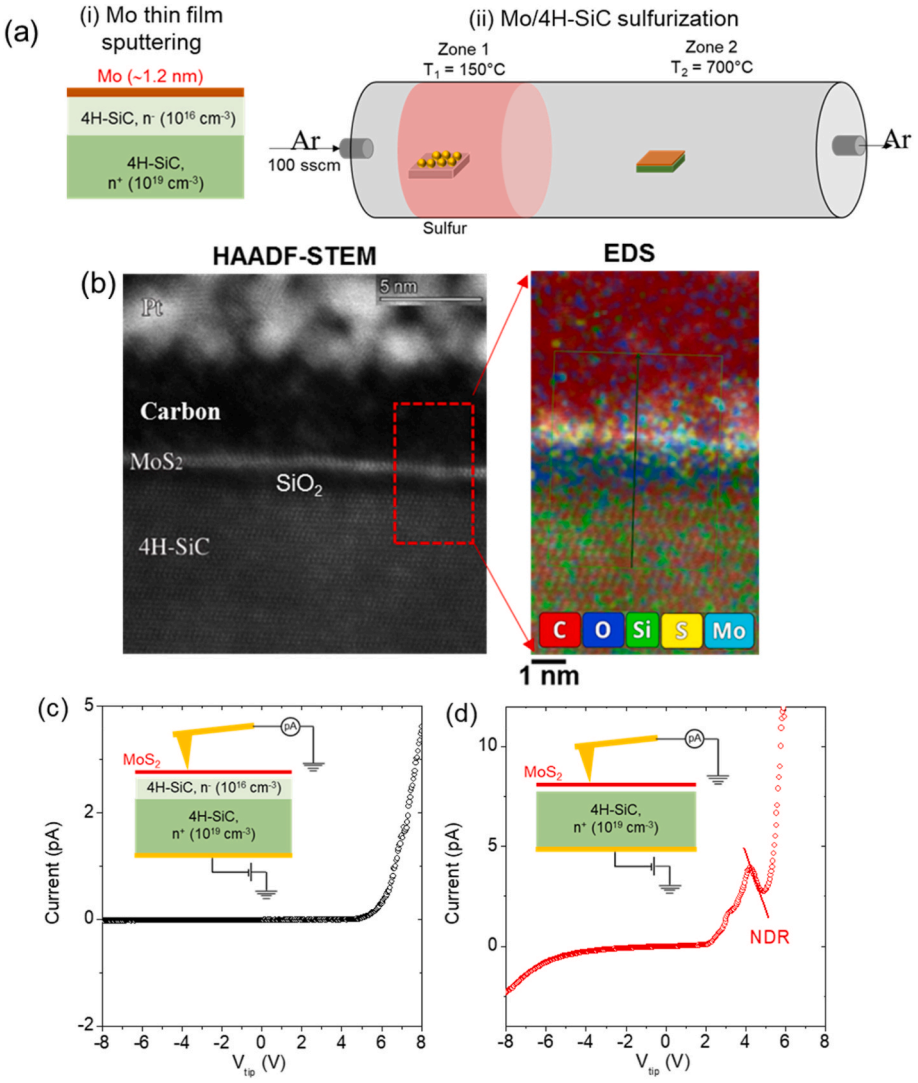

Fig. 6. (a) Schematic illustration of the two-steps CVD approach for MoS_2 growth on SiC, consisting in the deposition of an ultra-thin Mo film, followed by sulfurization in a two-heating zones furnace. (b) Cross sectional HAADF-STEM image and EDS chemical map, showing the formation of 1L MoS_2 on 4H-SiC. Representative current voltage characteristics of MoS_2 heterojunction with n^- 4H-SiC epitaxy (c) and n^+ doped SiC substrate (d), measured by the metal tip of CAFM. While a rectifying behavior with high positive onset voltage is observed for the p^+ MoS_2/n^- SiC junction, a larger reverse current and the presence of negative differential resistance (NDR) at positive bias is observed in the case of the p^+ MoS_2/n^+ SiC junction. Figures adapted from Ref. [37].

thermionic-field-emission was the dominant transport mechanism for the MoS_2/n^+ SiC junctions, resulting in a significantly lower effective barrier Φ_B=(0.31 ± 0.01) eV and higher ideality factor.

3. Open research directions in materials integration

3.1. van der Waals epitaxy of GaN and Ga_2O_3 on Epi-Gr/SiC(0001)

GaN and related AlGaN/GaN heterostructures are materials of choice for high power and high frequency devices, such us the high electron mobility transistors (HEMTs), currently employed in strategic fields like telecommunications (5G technology). Typically, these devices are fabricated using micrometer-thick GaN films heteroepitaxially grown on foreign substrates, such as sapphire, silicon or silicon carbide. In fact, despite many recent advances in the homoepitaxial GaN growth on free-standing GaN substrates, the cost of bulk GaN wafers still remains too high to be an industrially viable solution. As a matter of fact, hetero-epitaxial GaN layers are affected by a high density of defects (such as the threading dislocations) originating from the in-plane lattice mismatch between GaN and the substrates. The common strategy to reduce the defects' density reaching GaN surface (i.e. the device active region) is to grow optimized AlN buffer layer structures on the substrate to accommodate the strain. However, even using this approach, the typical density of threading dislocations for heteroepitaxial GaN is in the range from 10^7 to 10^9 cm^{-2}, with respect to a density of 10^3 - 10^6 cm^{-2} for homoepitaxial GaN [78].

These issues related to lattice constant mismatch are typical of the classical epitaxy approaches, relying on the formation of strong (e.g. covalent) bonds between the dangling bonds of the crystalline substrate and the atoms of the epitaxial material. Recently, the availability of 2D layered materials on large area allowed to explore a new epitaxial growth approach, i.e. the van der Waals (vdW) epitaxy, which is driven by the weak interaction between the dangling-bond-free surface of the 2D materials and the adatoms. In this context, Epi-Gr represents an ideal 2D interlayer to promote the van der Waals epitaxy on SiC(0001). In particular, Kim et al. [79] first demonstrated the direct growth of micrometer-thick single crystalline GaN on Epi-Gr/SiC, without the need of any AlN buffer layer, by an optimized MOCVD process consisting of GaN nucleation (at $T_1 = 1100$ °C) and growth (at $T_2 = 1250$ °C). Fig. 7(a) reports the surface morphology of as-grown Epi-Gr on SiC, characterized by flat terraces, ~10 μm wide, separated by parallel steps. Fig. 7(b), collected after the first MOCVD step at $T_1 = 1100$ °C, demonstrates the preferential nucleation of GaN along the step edges. On the other hand, the formation of a continuous and smooth GaN films was obtained after the second growth step at $T_2 = 1250$ °C (Fig. 7(c)). The higher temperature resulted in a higher surface mobility of adatoms on Epi-Gr terraces, enabling the lateral growth of GaN starting from the nuclei at step edges. The final thickness of the uniform GaN film grown under these conditions was ~2.5 μm, as shown by the low-magnification cross-sectional TEM in Fig. 7(d).

Well aligned, ordered crystal lattices of GaN, Epi-Gr and 4H-SiC is observed in the high resolution TEM analysis of the interface. Finally, Fig. 7(e) shows a typical plan view TEM image of the GaN film, from which a density of threading dislocations ~4×10^8 cm^{-2} was evaluated. Hence, even without using any buffer layer, vdW epitaxy on Epi-Gr allowed to achieve a GaN crystalline quality similar to the one obtained via conventional AlN-buffer-assisted GaN epitaxy on SiC or sapphire substrates.

One of the key advantages of the presence of the few-layer Epi-Gr between 4H-SiC and the grown GaN film is the possibility to detaching this film from the original substrate and transferring it to host substrates, including flexible ones (e.g. plastic ones). An effective approach to separate the GaN membrane from Epi-Gr is to deposit a thin Ni films on GaN and to exploit the stress induced by this layer on the underlying GaN membrane to overcome the weak vdW bond with Epi-Gr. After the separation of GaN, the Epi-Gr/SiC(0001) substrate can be reused for another vdW epitaxy growth, and this cycle can be repeated for large number of times, becoming an economically viable solution for the production of high crystalline quality free standing-GaN membranes.

The van der Waals epitaxy approach is not limited to GaN growth, as it has been recently extended to the growth of another technologically relevant ultra-wide bandgap semiconductor, the gallium oxide (β-Ga_2O_3), on Epi-Gr/SiC(0001) surface [80]. Moreover, the β-Ga_2O_3 membrane was effectively detached from Epi-Gr using a Ni stressor, and it was used for the fabrication of a flexible solar-blind deep-UV photodetector.

In addition to graphene, also the layered MoS_2 and WS_2 have been recently proposed as templates for GaN growth [81,82], thanks to the

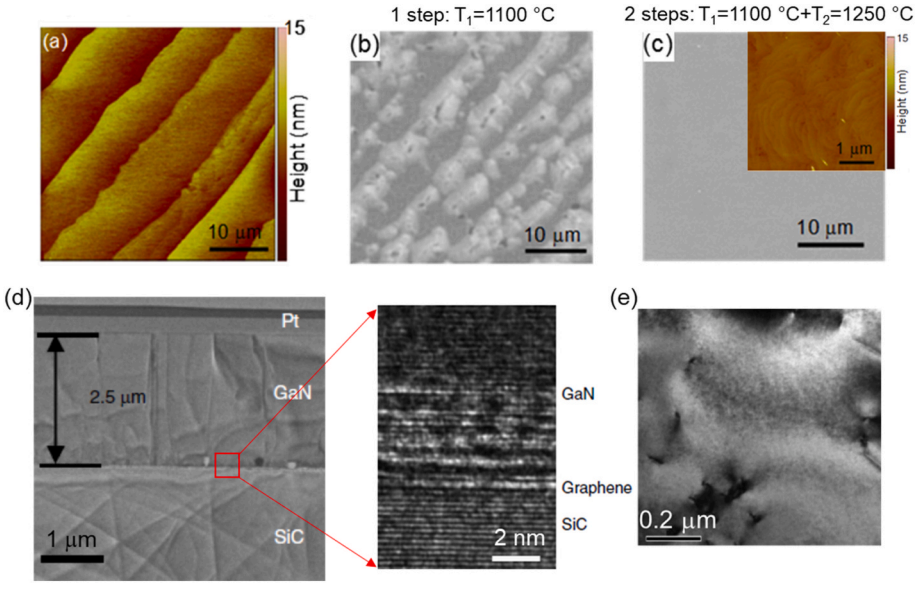

Fig. 7. (a) AFM surface morphology of as-grown Epi-Gr on SiC(0001). Plan-view SEM image of GaN grown on Epi-Gr by 1-step MOCVD at 1100 °C (b) and by 2-steps MOCVD: nucleation at $T_1 = 1100$ °C and growth at $T_2 = 1250$ °C (c). (d) Cross-sectional TEM of the 2.5 μm thick GaN membrane directly grown on Epi-Gr/SiC and high resolution TEM image on the GaN/Epi-Gr/SiC interface region. (e) Plan view TEM image of the released GaN membrane, allowing to estimate a density of threading dislocations from ~4×10^8 cm^{-2} to ~2.3×10^9 cm^{-2}, comparable to the one of GaN grown on SiC with AlN buffer layer. Figures adapted from Ref. [79].

very low lattice mismatch with respect to GaN (as illustrated Fig. 5). To date, the direct growth of nearly unstrained GaN films has been obtained by metalorganic vapor phase epitaxy (MOVPE) on mechanically exfoliated multilayer WS_2 and MoS_2 [81] and by molecular beam epitaxy (MBE) on single layer MoS_2 deposited by CVD on sapphire [82]. Although MoS_2 and WS_2 have been not yet used as interlayer for vdW epitaxy on SiC, the literature results reported so far indicate this as a viable approach.

3.2. Synthesis of novel 2D semiconductors on SiC

In the last few years, advanced approaches have been explored to grow new forms of 2D materials not existing in nature on the SiC surface. These include the 2D group-III Nitrides (i.e. 2D-GaN [83,84], 2D-InN [85] and 2D-AlN [86,87]), 2D oxides (2D-InOx [88] and 2D-GaOx [89]) and, more recently, 2D-SiN [90] and 2D-SiC [91].

The formation 2D layers of GaN with hexagonal buckled structure was obtained for the first time by Al Balushi et al. [83] by the confinement epitaxy at Epi-Gr/SiC interface within a metal organic chemical vapor deposition (MOCVD) reactor using trimethylgallium (TMG) and ammonia (NH_3) as the Ga and N precursors (see the schematic illustration in Fig. 8(a)). The compositional and structural properties of the 2D GaN intercalated in the confined space between bilayer graphene and SiC were investigated by EDX (Fig. 8(b)) and aberration corrected STEM analyses (Fig. 8(c) and (d)). Following these pioneering studies, the confinement epitaxy MOCVD approach has been adopted by other research groups and its application has been extended to the growth of 2D-InN using trimethylindium (TMIn) and NH_3 precursors [85], and of 2D-AlN using trimethylaluminum (TMA) and NH_3 precursors [86]. Starting from the 2D-InN growth conditions, Kakanakova et al. obtained the formation of 2D-InOx by intentionally leaving oxygen residues in the MOCVD chamber [88]. More recently, the formation of non stoichiometric 2D-GaO_x has been obtained by intercalation of Ga atoms at Epi-Gr/SiC interface, followed by ex-situ oxidation in air at room temperature [89], whereas crystalline monolayer GaO_2 and bilayer Ga_2O_3 with ferroelectric wurtzite structure were formed via subsequent high-temperature O_2 annealing [89].

A noteworthy feature of the obtained 2D group III Nitrides and oxides is a larger energy bandgap than the bulk counterpart materials, due to a quantum confinement effect. As an example, an energy bandgap value $E_g \approx 4.9$ eV has been experimentally determined for 2D-GaN using optical measurements [83] (larger than the 3.4 eV value for bulk GaN), whereas a bandgap of $E_g = 2.0 \pm 0.1$ eV has been measured by scanning tunneling spectroscopy for 2D-InN [85] (as compared to the 0.7 eV value for bulk InN). Furthermore, by using current transport measurements with C-AFM, an energy bandgap $E_g = 4.1 \pm 0.1$ eV has been evaluated for 2D-InO_x [88], and $E_g = 6.6 \pm 0.6$ eV for 2D-Ga_2O_3 [89], which are significantly larger with respect to the values for the In_2O_3 ($E_g = 2.7$ eV) and β-Ga_2O_3 (4.8 eV) bulk counterparts.

A different approach has been recently used to obtain the growth of 2D SiC, i.e. the deposition of an ultrathin (<3 nm) epitaxial films of transition metal carbides (TaC, NbC) on the 4H-SiC(0001) surface, followed by annealing at high temperature (>1700 °C) in Ar ambient [91]. Uniform 2D-SiC layers were observed on the TaC or NbC surface, after this annealing process. Due to the high thermal stability of these metal carbides even at these high temperatures, the proposed formation mechanism of 2D-SiC was the decomposition of the buried SiC surface, followed by the diffusion of Si and C though the TaC (or NbC) film, and segregation of the epitaxial 2D SiC on its surface [91]. Furthermore, density functional theory (DFT) calculations and initial experimental evidences by ARPES indicated a direct bandgap of 2.5 eV for 2D-SiC, which can make this material interesting for optoelectronic applications.

4. Device applications of 2D materials on SiC

4.1. RF transistors

Due to its high carrier mobility, Epi-Gr grown on semi-insulating (SI) SiC has been considered for the fabrication of high frequency transistors. The first report of a top-gated graphene RF transistor on wafer scale Epi-Gr on SI 6H-SiC(0001), as illustrated Fig. 9(a), dates back to 2010 [28]. The transfer characteristic of the device (Fig. 9(b) left scale) show the

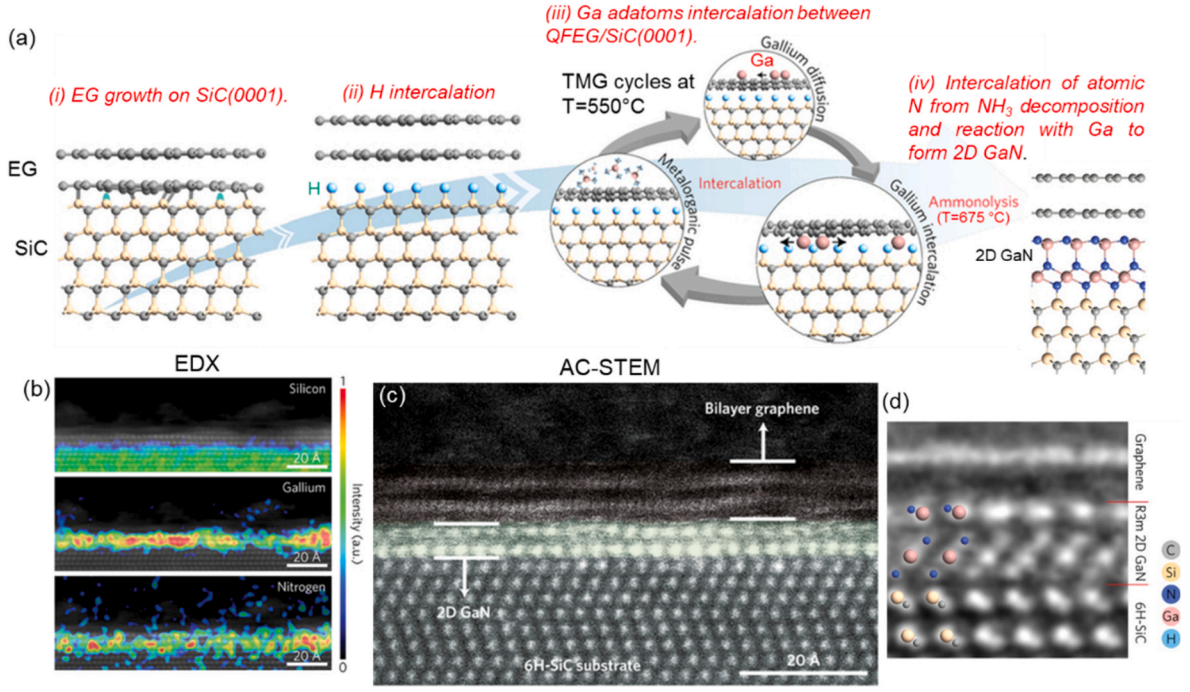

Fig. 8. (a) Schematic illustration of the process-flows for confined epitaxy of 2D GaN at the interface between Epi-Gr and SiC, using TMGa and NH_3 MOCVD precursors. (b) Cross-sectional EDX maps of Si, Ga, and N distribution in the graphene/2D-GaN/SiC heterostructure (c) HAADF-STEM image of the same heterostructure and (d) atomic resolution image of the atomic distribution. Figures adapted with permission from Ref. [83].

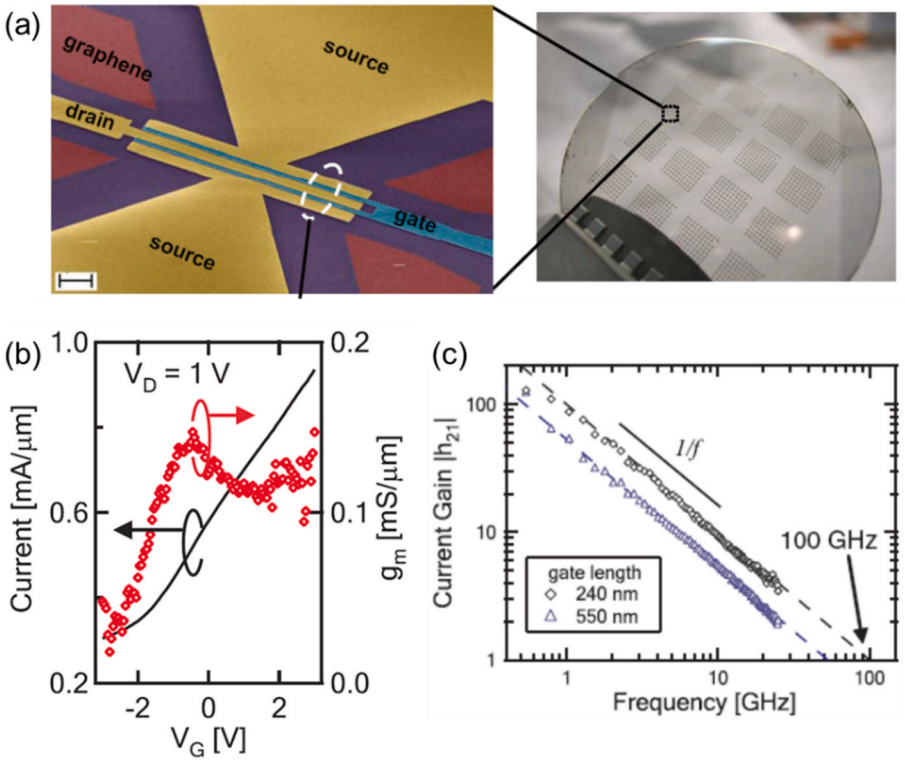

Fig. 9. (a) SEM image of a top-gated Epi-Gr transistor for RF applications fabricated in a semi-insulating 4H-SiC wafer. (b) Transfer characteristic I_D-V_G (left scale) and transconductance g_m-V_G (right scale) of the transistor. (c) Current gain $|h_{21}|$ vs frequency of transistors with gate length of 240 nm and 550 nm. The cut off frequency of the device is evaluated by extrapolation of the frequency for which $|h_{21}| = 1$. Figures adapted with permission from Ref. [28].

typical n-type behavior of Epi-Gr on SiC, and a transconductance peak $g_m = 0.12$ mS/μm. This first demonstrator reached a very high cut-off frequency $f_T = 100$ GHz for a gate length $L_g = 240$ nm [28], as illustrated in Fig. 9(c).

Later-on, the performances of these RF transistors were further improved, after identifying some of the factors limiting the carrier mobility of Epi-Gr on SiC(0001). As an example, a significant reduction of the mobility is due to the electron scattering in graphene at the step-edges of SiC surface [47,53]. An improved transconductance $g_m = 0.3$ mS/μm and a cut-off frequency $f_T = 210$ GHz (at $L_g = 210$ nm), was simply achieved by fabricating the transistors with the Epi-Gr channel residing within single SiC(0001) terraces, thus avoiding step-edges scattering effects [92]. Besides the cut-off frequency f_T (i.e., the frequency at which the current gain is unity), another important figure of merit for RF transistors is the maximum oscillation frequency f_{max} (i.e., the frequency at which the power gain is unity). As a matter of fact, reaching high values for both f_T and f_{max} is important for practical applications of RF transistors. However, despite the very high demonstrated f_T values, transistors based on Epi-Gr grown on Si terminated SiC typically exhibit very poor f_{max}, due to the difficulty of achieving current saturation in the output characteristics. In this context, some authors reported on the possibility of reaching $f_T = 110$ GHz and $f_{max} = 70$ GHz in RF transistors with $L_g = 100$ nm fabricated on monolayer Epi-Gr grown on the C terminated face of SiC [93]. This remarkable f_{max} value was explained in terms of the higher mobility of Epi-Gr on the (000–1) face and the electron scattering by the substrate phonons, which allowed to approach output characteristics saturation. More recently, $f_{max}/f_T > 1$ (with $f_{max} = 120$ GHz and $f_T = 70$ GHz) have been obtained in a RF transistor with the channel ($L_g = 60$ nm) made of QFSBG on SiC (0001) [94], obtained by annealing the monolayer Epi-Gr in molecular hydrogen at 900 °C. The bilayer graphene showed p-type doping (holes density 1.3×10^{13} cm^{-2}) and carrier mobility $\mu = 3200$ cm^{2}V^{-1}s^{-1}. Such bilayer graphene RF transistors have been recently demonstrated to be able to operate at temperatures as high as 200 °C [95].

The availability of wafer scale Epi-Gr on SiC allowed not only the demonstration of single RF devices, but also the demonstration of integrated circuits with advanced functionalities [96], which have been considered for high data rate telecommunications [97].

Currently, a key aspect to further improve the performances of Epi-Gr transistors is represented by the interface quality and thickness scalability of high-k gate dielectrics (such as Al_2O_3 or HfO_2). The growth of these insulating films on graphene is commonly obtained by the atomic layer deposition (ALD) technique. Due to the highly inert nature of graphene surface, the initiation of the ALD growth typically requires the pre-deposition of a seed-layer (e.g. a thin Al or AlO_x film or a polymer thin film), which however affects the final electrical quality of the high-k/graphene interface and ultimately limits the scalability of the dielectric thickness. Hence, the direct ALD growth of high-k dielectrics on graphene surface is highly desirable for the ultimate scaling of transistor channel [98]. In this context, recent investigations on the initial stages of ALD growth of Al_2O_3 onto Epi-Gr/4H-SiC(0001) surface revealed an enhanced Al_2O_3 nucleation on the monolayer Epi-Gr regions, promoted by the electrostatic interaction of the ALD precursors with the charges at buffer layer/SiC interface. A similar substrate-enhanced ALD nucleation phenomenon of Al_2O_3 and HfO_2 during thermal ALD has been also observed on monolayer graphene and on monolayer MoS_2 supported by metal substrates [99–101]. By exploiting this phenomenon, the formation of uniform and ultra-thin (3–4 nm) Al_2O_3 films been achieved on the surface of monolayer Epi-Gr after only 80 cycles of thermal ALD at 200 °C [102,103]. Such findings are extremely promising for further scaling in Epi-Gr RF transistors.

4.2. Quantum Hall resistance standard

Due to its excellent electronic transport properties, Epi-Gr on SiC (0001) has been intensively investigated in the last decade to implement a quantum Hall resistance standard (QHRS) in replacement to the

commonly used one based on GaAs/AlGaAs heterostructures [29,30]. The quantum Hall effect (QHE) is a macroscopic quantum phenomenon occurring in a 2DEG Hall bar device placed under a magnetic field. It manifests in the quantization of the (transverse) electrical resistance as $R_H = h/(nq^2)$, where h is the Planck constant, q is the electron charge and n is an integer. This fundamental relation provides a universal and reproducible electrical resistance reference for metrology. The widely used QHRS, based on GaAs/AlGaAs heterostructures, typically require very high magnetic flux densities (B≈10 T), achievable only with superconducting cryomagnetic systems, low temperatures (T ≈1.3 K, i.e. below liquid helium temperature) and low measurement currents (I < 10 μA) in order to achieve an accuracy of R_H within 1×10^{-9}. More relaxed operational conditions in terms of B, T, and I values are highly desirable to reduce calibration costs, leading to a broad dissemination of QHRS beyond national metrology institutes and to industrial stakeholders. In this context, the QHRS based on Epi-Gr grown on SiC(0001) allowed to measure a plateau of R_H (with 1×10^{-9} accuracy) down to significantly lower magnetic field (B = 4 T), at an operating temperature T = 1.3 K and a current I = 0.1 μA, [30]. This represented a clear advancement toward the wider use of QHRS outside specialized metrology institutes.

4.3. THz detectors

The high electron mobility 2DEG on large area provided by Epi-Gr on SiC has been also exploited for photodetection in the THz frequency range. The interest in reliable THz detectors operating at room temperature is motivated by the growing applications in strategic fields like biomedical diagnostics, security controls, and industrial process monitoring.

Generally, photodetectors convert incoming light into an electrical signal. A first approach to implement a THz detector with graphene has been to couple a top-gated Epi-Gr field effect transistor to a log-periodic circular-toothed antenna [104], as illustrated in Fig. 10(a). More specifically, the gate and source of the transistor were connected to the two lobes of the antenna, whereas the drain was connected to a metal line. A 35 nm thick HfO_2 deposited by ALD was used as the gate dielectric, and the gate length was L_g = 300 nm. Fig. 10(b) shows the measured photovoltage ΔU as a function of the frequency of the incident radiation in the range from 230 to 390 GHz, for two different polarization angles of the radiation with respect to the axis of the antenna. The maximum photovoltage was recorded when the polarization was parallel to the antenna axis, with the peak frequencies related to the geometry of the antenna. A maximum responsivity R = 0.25 V/W and minimum noise-equivalent-power NEP = 80 nW/Hz$^{1/2}$ was achieved at 263 GHz and 325 GHz frequencies, whereas R = 0.15 V/W and NEP = 160 nW/Hz$^{1/2}$ were obtained at 295 GHz and 353 GHz. At room temperature, the conversion of the incoming THz photons into electrical signal by the graphene FET is typically ruled by three main mechanisms: bolometric (associated to graphene channel conductivity variation due to photon absorption), thermoelectric (related to a photovoltage generated by a temperature gradient within the graphene channel), and plasmonic (due to rectification of the THz-induced ac current in the channel of the transistor). The two latter mechanisms have been demonstrated to play a competitive role in the determination of the photoresponse for this specific device [104].

The performances of this kind of THz detectors have been further improved by enhancing the Epi-Gr mobility, and scaling the channel length and the top-gate dielectric thickness. As an example, a voltage responsivity R = 30 V/W and NEP = 51 pW/Hz$^{1/2}$ at 0.33 THz frequency have been recently reported using H-intercalated QFSBG/SiC(0001) with μ = 3000 cm^{2}V^{-1}s^{-1} as the channel material in a device with L_g = 145 nm and aluminium oxide thickness of ~7 nm [105]. Furthermore, several strategies to enhance THz radiation response of Epi-Gr on SiC have been explored, including geometric patterning of graphene micro-stripes [106,107], or by nano-patterning of graphene quantum dots [108].

Besides top-gated Epi-Gr FET on semi-insulating SiC, recently an Epi-Gr/n-type SiC Schottky diode coupled to an antenna proved to be very effective for THz radiation detection up to a frequency of 580 GHz (limited only by the RC circuitry), with a maximum responsivity of 1.1 A/W at 90 GHz [109].

4.4. UV photodetectors based on Epi-Gr and MoS_2 on SiC

Due to its wide band gap of 3.26 eV, combined to high thermal conductivity, chemical inertness, and radiation hardness, 4H-SiC represents an excellent semiconductor material for the fabrication of visible-blind UV photodetectors, which are able to operate also under harsh environments [110]. For the spectral range between 200 and 400 nm, visible-blind SiC based photodetectors demonstrated very low leakage current and high responsivity even at high temperatures [111]. A common approach to implement SiC-based UV photodetectors has been fabricating interdigit Schottky electrodes on its surface and exploiting lateral pinch-off of bare SiC between these contacts [112]. However, in this configuration only a fraction of the device active area is available for photodetection. Alternatively, conductive oxides (like ITO) or semi-transparent thin (<20 nm) metal films (such as Ni, Ni/Au, Ti, Ti/W) [113,114] have been employed to collect photo-generated charge carriers. However, most of these films exhibit an inherent low optical transmittance (<80%) in the UV regime below 400 nm, due to high surface reflection and absorption. Differently, due to its peculiar energy bandstructure, monolayer graphene transmittance in the 200–400 nm wavelength range is >90% [6], making it a promising candidate as transparent and conductive electrode for UV photodetectors. In particular, different Epi-Gr/SiC UV photodetectors configurations have been demonstrated so far. A first example is a graphene/SiC/graphene lateral photodetector with interdigited monolayer Epi-Gr contacts grown on the

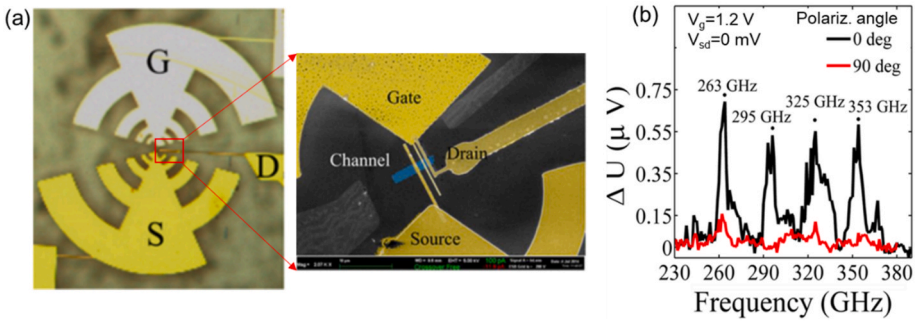

Fig. 10. (a) Optical image of a log-periodic circular-toothed antenna, with the lobes connected to the source and gate of an Epi-Gr field effect transistor, while the drain was a metal line. (b) Measured photovoltage as a function of the incident radiation frequency at V_g = 1.2 V, V_{sd} = 0 mV, and for 0° and 90° polarization with respect to the antenna axis. Figures adapted with permission from Ref. [104].

(0001) face of semi-insulating 4H-SiC [31], as illustrated in Fig. 11(a). When the UV light impinges on the device surface, the photons penetrate into SiC substrate both through the transparent Epi-Gr electrodes and uncovered SiC surface in between these electrodes. As illustrated in the energy band diagram in Fig. 11(b), electron–hole pairs are created in the SiC depletion region. Under applied bias V_b, electrons and holes are separated and collected at the two interdigited Epi-Gr electrodes, working as the cathode and anode, respectively, giving rise to a photocurrent (I_p) more than two orders of magnitude higher than the device dark current (I_d). Typical dark current (I_d vs.V_b) and photocurrent (I_p vs. V_b) characteristics under illumination with an UV laser wavelength $\lambda = 254$ nm with a power $P = 0.3$ mW are reported in Fig. 11(c), while Fig. 11(d) shows the bias dependent responsivity $R=(I_p-I_d)/(S \times P)$, with P the lase power and S the detector area, for different UV wavelengths (i.e., 254 nm, 311 nm, and 365 nm) [31]. The correlation between the photoresponse performances of Epi-Gr/SiC/Epi-Gr lateral UV detectors and the device geometry, number of graphene layers and graphene carrier density has been also investigated [115]. Furthermore, top-gated planar Epi-Gr/SiC devices have been recently employed to achieve high UV responsivity by electric field modulation of graphene doping [116].

Besides lateral Epi-Gr/SiC devices, vertical UV photodetector configurations (based on the Schottky junction between a uniform graphene layer and SiC) have been also demonstrated, where bias/current are applied/collected in a front-to-back configuration [117,118]. As an example, a device based on few layer Epi-Gr Schottky contacts grown on n-type 6H-SiC(000–1) has been reported, showing tunable responsivity over three orders of magnitude and response time over seven orders of magnitude (from 10^{-1} to 10^{-8} s) by increasing the front-to-back bias reverse bias in the range from 0 to −5 V [117]. Alternatively, a vertical photodetector structure based on the junction of few-layer Epi-Gr on the (0001) surface of a p^-/n^+ SiC epitaxial stack, with p^+ implanted terminations, allowed to minimize reverse current leakage and achieve a maximum responsivity of 200 mW/A at a photon wavelength of 310 nm [118].

Besides semimetallic graphene, also semiconducting MoS_2 has been recently considered as a top electrode to fabricate SiC photodetectors [39,119], The reported demonstrators were typically planar devices, formed by continuous monolayer or few layers MoS_2 (transferred or directly grown on SiC), with top source/drain metal contacts [39], as schematically illustrated in Fig. 12(a)). These MoS_2/SiC detectors exhibit good responsivity both in visible range, due to photogenerated electron-hole pairs in the low bandgap MoS_2 film (see Fig. 12(b)), and in the UV range, due to the combined effects of band-to-band photogeneration in the SiC depletion region and efficient carrier collection across the MoS_2/SiC heterojunction (see Fig. 12(c)). Typical responsivity values vs the incident power under visible ($\lambda = 660$ nm) and UV ($\lambda = 365$ nm) wavelength ranges under the same polarization of the source/drain electrodes onto MoS_2 are reported in Fig. 12(d) and (e).

5. Summary

The state-of-the art methods for scalable growth of graphene and MoS_2 on hexagonal SiC have been reviewed. In particular, high temperature decomposition of SiC or CVD growth with propane carbon source are well assessed methods to obtain uniform Epi-Gr on the SiC (0001) with precise control of the thickness down the monolayer. Furthermore, hydrogen intercalation at buffer layer/SiC interface proved an efficient way to tailor both Epi-Gr electronic properties (doping, mobility) and the vertical current injection across graphene/SiC interface from Ohmic to Schottky contacts, thus allowing the implementation of monolithic Epi-Gr/SiC devices. Significant progresses have been also carried out in the last years in the growth of MoS_2 on SiC by scalable approaches like single and two-steps CVD or by PLD. Furthermore, Epi-Gr on SiC has been employed as an interlayer to promote van der Waals epitaxy of GaN or Ga_2O_3 on SiC substrates. New research directions recently opened, such as the growth of 2D forms of group-III nitrides (2D-GaN, InN and AlN) or oxides (InOx, GaOx) by confined epitaxy at Epi-Gr/SiC interface. A discussion of recent electronics/optoelectronics applications Epi-Gr/SiC or MoS_2/SiC systems, specifically for high frequency electronics, quantum metrology, THz and UV detectors, has been finally provided. This work can be a useful guide for silicon carbide community on these open research directions.

CRediT authorship contribution statement

Filippo Giannazzo: Writing – original draft, Supervision, Funding acquisition, Conceptualization. **Salvatore Ethan Panasci:** Writing –

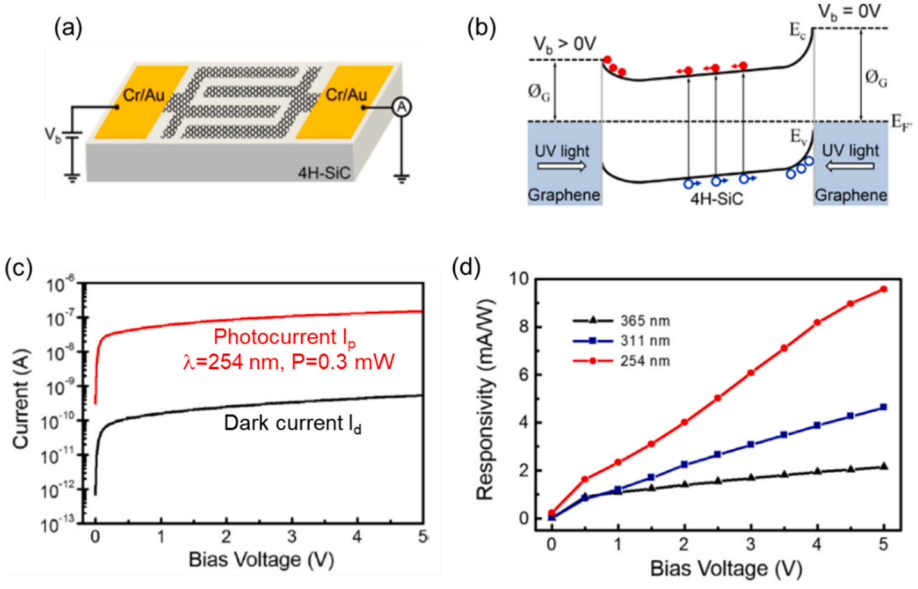

Fig. 11. (a) Schematic of the UV photodetector with interdigitated 1L Epi-Gr contact fingers onto 4H-SiC. (b) Illustration of energy band diagram of the device and its operating principle under UV illumination. (c) Dark current and photocurrent under 254 nm UV illumination with 0.3 mW power, measured as a function of bias voltage. (d) Responsivity of the device as a function of bias voltage under illumination with different UV wavelengths (254 nm, 311 nm and 365 nm). Figures adapted with permission from Ref. [31].

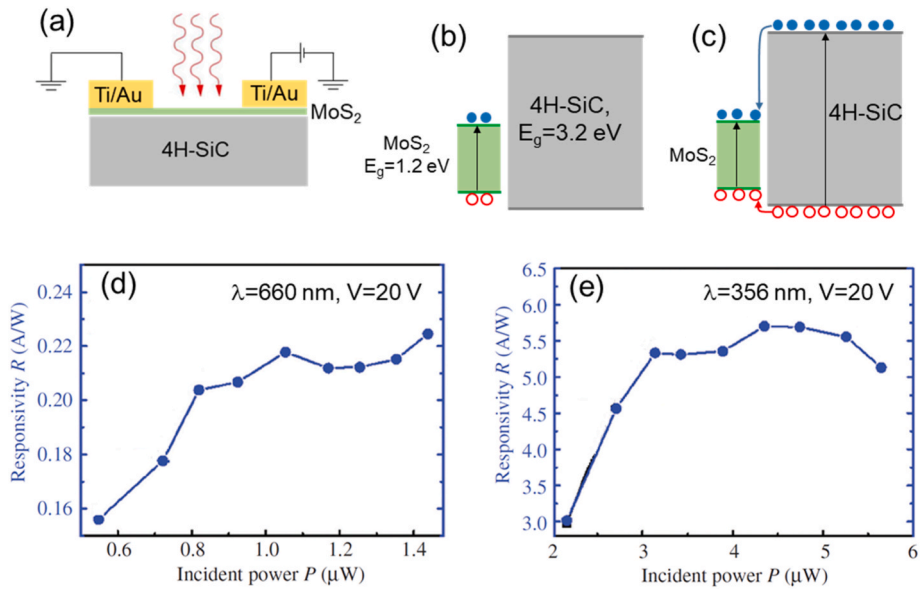

Fig. 12. (a) Schematic of a few layers MoS_2/4H-SiC photodetector with interdigitated metal contacts. Illustration of MoS_2/4H-SiC energy band alignment and carrier excitation under illumination with (b) visible and (c) UV light. (d) Device responsivity (at a bias V = 20 V) under illumination with 660 nm (d) and 365 nm (e) wavelengths as a function of incident power. Figures adapted with permission from Ref. [39].

review & editing. **Emanuela Schilirò:** Writing – review & editing. **Antal Koos:** Writing – review & editing. **Béla Pecz:** Writing – review & editing, Supervision, Funding acquisition.

Declaration of competing interest

The authors declare that they have no known competing financial interests or personal relationships that could have appeared to influence the work reported in this paper.

Data availability

Data will be made available on request.

Acknowledgements

F. Roccafore, P. Fiorenza, G. Greco, R. Lo Nigro, M. Vivona, G. Nicotra, G. Sfuncia, I. Deretzis, A. La Magna (CNR-IMM, Catania, Italy), S. Agnello, M. Cannas, F. M. Gelardi (University of Palermo, Italy), Y. Cordier, A. Michon, M. Al Khalfioui (CNRS-CRHEA, France), M. Spankova, S. Chromik (IEE-SAS, Bratislava, Slovakia), R. Yakimova and A. Kakanakova Gueorguieva (University of Linkoping, Sweden) are acknowledged for useful discussions. This work was supported by MUR in the framework of the FlagERA JTC 2019 project ETMOS. Funding for travels from CNR/HAS (2023-25) bilateral project GHOST-III is acknowledged. B.P acknowledges funding from the national project TKP2021-NKTA-05. The authors from CNR acknowledge Next-Generation EU funding through the MUR - PRIN2022 project "2DIntegratE" (2022RHRZN2) and the MUR - PNRR project "SAMOTHRACE" (ECS00000022).

References

[1] K.S. Novoselov, A.K. Geim, S.V. Morozov, D. Jiang, Y. Zhang, S.V. Dubonos, I. V. Grigorieva, A.A. Firsov, Electric field effect in atomically thin carbon films, Science 306 (2004) 666.
[2] C. Berger, Z. Song, X. Li, X. Wu, N. Brown, C. Naud, D. Mayou, T. Li, J. Hass, A. N. Marchenkov, E.H. Conrad, P.N. First, W.A. de Heer, Electronic confinement and coherence in patterned epitaxial graphene, Science 312 (2006) 1191–1196.
[3] A.K. Geim, I.V. Grigorieva, Van der Waals heterostructures, Nature 499 (2013) 419–425.
[4] J. Zhou, L. Shen, M.D. Costa, K.A. Persson, S.P. Ong, P. Huck, Y. Lu, X. Ma, Y. Chen, H. Tang, Y.P. Feng, 2DMatPedia, an open computational database of two-dimensional materials from top-down and bottom-up approaches, Sci. Data 6 (2019) 86.
[5] Q.H. Wang, K.K. Zadeh, A. Kis, J.N. Coleman, M.S. Strano, Nat. Nanotechnol. 7 (2012) 699.
[6] H. Liu, A.T. Neal, Z. Zhu, Z. Luo, X. Xu, D. Tománek, P.D. Ye, Phosphorene: an unexplored 2D semiconductor with a high hole mobility, ACS Nano 8 (2014) 4033–4041.
[7] K. Watanabe, T. Taniguchi, H. Kanda, Direct-bandgap properties and evidence for ultraviolet lasing of hexagonal boron nitride single crystal, Nat. Mater. 3 (2004) 404–409.
[8] T. Roy, et al., Field-effect transistors built from all two-dimensional material components, ACS Nano 8 (2014) 6259–6264.
[9] F. Withers, et al., Light-emitting diodes by band-structure engineering in van der Waals heterostructures, Nat. Mater. 14 (2015) 301.
[10] G. Ruhl, S. Wittmann, M. Koenig, D. Neumaier, The integration of graphene into microelectronic devices, Beilstein J. Nanotechnol. 8 (2017) 1056–1064.
[11] C. Zeng, E.B. Song, M. Wang, S. Lee, C.M. Torres, J. Tang, B.H. Weiller, K. L. Wang, Vertical graphene-base hot-electron transistor, Nano Lett. 13 (2013) 2370.
[12] G. Fisichella, G. Greco, F. Roccaforte, F. Giannazzo, Current transport in graphene/AlGaN/GaN vertical heterostructures probed at nanoscale, Nanoscale 6 (2014) 8671–8680.
[13] F. Giannazzo, G. Fisichella, G. Greco, A. La Magna, F. Roccaforte, B. Pecz, R. Yakimova, R. Dagher, A. Michon, Y. Cordier, Graphene integration with nitride semiconductors for high power and high frequency electronics, Phys. Status Solidi A 214 (2017) 1600460.
[14] A. Zubair, A. Nourbakhsh, J.-Y. Hong, M. Qi, Y. Song, D. Jena, J. Kong, M. Dresselhaus, T. Palacios, Hot electron transistor with van der Waals base-collector heterojunction and high-performance GaN emitter, Nano Lett. 17 (2017) 3089.
[15] F. Giannazzo, G. Greco, E. Schilirò, R. Lo Nigro, I. Deretzis, A. La Magna, F. Roccaforte, F. Iucolano, S. Ravesi, E. Frayssinet, A. Michon, Y. Cordier, High-Performance graphene/AlGaN/GaN Schottky junctions for hot electron transistors, ACS Appl. Electron. Mater. 1 (2019) 2342–2354.
[16] D. Ruzmetov, K. Zhang, G. Stan, B. Kalanyan, G.R. Bhimanapati, S.M. Eichfeld, R. A. Burke, P.B. Shah, T.P. O'regan, F.J. Crowne, A.G. Birdwell, J.A. Robinson, A. V. Davydov, T.G. Ivanov, Vertical 2D/3D semiconductor heterostructures based on epitaxial molybdenum disulfide and gallium nitride, ACS Nano 10 (2016) 3580.
[17] S.E. Panasci, I. Deretzis, E. Schilirò, A. La Magna, F. Roccaforte, A. Koos, M. Nemeth, B. Pécz, M. Cannas, S. Agnello, F. Giannazzo, Interface properties of MoS_2 van der Waals heterojunctions with GaN, Nanomaterials 14 (2024) 133.
[18] T. Kimoto, J.A. Cooper, Fundamentals of Silicon Carbide Technology, John Wiley & Sons, Singapore, 2014.
[19] F. Roccaforte, P. Fiorenza, G. Greco, R. Lo Nigro, F. Giannazzo, F. Iucolano, M. Saggio, Emerging trends in wide band gap semiconductors (SiC and GaN) technology for power devices, Microelectron. Eng. 187–188 (2018) 66.
[20] F. La Via, D. Alquier, F. Giannazzo, T. Kimoto, P. Neudeck, H. Ou, A. Roncaglia, S. E. Saddow, S. Tudisco, Emerging SiC applications beyond power electronic devices, Micromachines 14 (2023) 1200.

[21] H. Ou, X. Shi, Y. Lu, M. Kollmuss, J. Steiner, V. Tabouret, M. Syväjärvi, P. Wellmann, D. Chaussende, Novel photonic applications of silicon carbide, Materials 16 (2023) 1014.

[22] S. Castelletto, A. Peruzzo, C. Bonato, B.C. Johnson, M. Radulaski, H. Ou, F. Kaiser, J. Wrachtrup, Silicon carbide photonics bridging quantum technology, ACS Photonics 9 (2021) 1434–1457.

[23] M. Mehregany, C.A. Zorman, N. Rajan, C.H. Wu, Silicon carbide MEMS for harsh environments, Proc. IEEE 86 (1998) 1594–1609.

[24] A.R. Kermany, G. Brawley, N. Mishra, E. Sheridan, W.P. Bowen, F. Iacopi, Microresonators with Q-factors over a million from highly stressed epitaxial silicon carbide on silicon, Appl. Phys. Lett. 104 (2014) 081901.

[25] S.E. Saddow, Silicon carbide technology for advanced human healthcare applications, Micromachines 13 (2022) 346.

[26] F. Giannazzo, I. Deretzis, A. La Magna, G. Nicotra, C. Spinella, F. Roccaforte, R. Yakimova, Nanoscale electrical and structural properties of epitaxial graphene interface with SiC(0001), in: Gemma Rius, Philippe Godignon (Eds.), Chapt. 4 of *Epitaxial Graphene On Silicon Carbide*, Jenny Stanford Publishing, 2018.

[27] J.S. Moon, D. Curtis, M. Hu, D. Wong, C. McGuire, P.M. Campbell, G. Jernigan, J. L. Tedesco, B. VanMil, R. Myers-Ward, C. Eddy Jr., D.K. Gaskill, Epitaxial-graphene RF field-effect transistors on Si-face 6H-SiC substrates, IEEE Electron. Device Lett. 30 (2009) 650–652.

[28] Y.-M. Lin, C. Dimitrakopoulos, K.A. Jenkins, D.B. Farmer, H.-Y. Chiu, A. Grill, P. Avouris, 100-GHz transistors from wafer-scale epitaxial graphene, Science 327 (2010) 662.

[29] A. Tzalenchuk, S. Lara-Avila, A. Kalaboukhov, S. Paolillo, M. Syvajarvi, R. Yakimova, O. Kazakova, T.J.B.M. Janssen, V. Falko, S. Kubatkin, Towards a quantum resistance standard based on epitaxial graphene, Nat. Nanotechnol. 5 (2010) 186–189.

[30] R. Ribeiro-Palau, F. Lafont, J. Brun-Picard, D. Kazazis, A. Michon, et al., Quantum Hall resistance standard in graphene devices under relaxed experimental conditions, Nat. Nanotechnol. 10 (2015) 965–971.

[31] E. Kusdemir, D. Özkendir, V. Fırat, C. Çelebi, Epitaxial graphene contact electrode for silicon carbide based ultraviolet photodetector, J. Phys. D Appl. Phys. 48 (2015) 095104.

[32] R. Pearce, T. Iakimov, M. Andersson, L. Hultman, A. Lloyd Spetz, R. Yakimova, Epitaxially grown graphene based gas sensors for ultra sensitive NO_2 detection, Sensor. Actuator. B 155 (2011) 451–455.

[33] C. Melios, V. Panchal, K. Edmonds, A. Lartsev, R. Yakimova, O. Kazakova, Detection of ultralow concentration NO_2 in complex environment using epitaxial graphene sensors, ACS Sens. 3 (2018) 1666–1674.

[34] Z. Tehrani, et al., Generic epitaxial graphene biosensors for ultrasensitive detection of cancer risk biomarker, 2D Mater. 1 (2014) 025004.

[35] S. Teixeira, et al., Epitaxial graphene immunosensor for human chorionic gonadotropin, Sensor. Actuator. B Chem. 190 (2014) 723–729.

[36] E.W. Lee II, L. Ma, D.N. Nath, C.H. Lee, A. Arehart, Y. Wu, S. Rajan, Growth and electrical characterization of two-dimensional layered MoS_2/SiC heterojunctions, Appl. Phys. Lett. 105 (2014) 203504.

[37] F. Giannazzo, S.E. Panasci, E. Schilirò, F. Roccaforte, A. Koos, M. Nemeth, B. Pécz, Esaki diode behavior in highly uniform MoS_2/silicon carbide heterojunctions, Adv. Mater. Interfac. 9 (2022) 2200915.

[38] J. Bradford, A. Zaganelli, D. Qi, N. Zebardastan, M. Shafiei, J. MacLeod, N. Motta, Substrate-mediated growth of oriented, vertically aligned MoS_2 nanosheets on vicinal and on-axis SiC substrates, Appl. Surf. Sci. 552 (2021) 149303.

[39] Y. Xiao, L. Min, X. Liu, W. Liu, U. Younis, T. Peng, X. Kang, X. Wu, S. Ding, D. W. Zhang, Facile integration of MoS_2/SiC photodetector by direct chemical vapor deposition, Nanophotonics 9 (2020) 3035–3044.

[40] F. Lan, Z. Lai, Y. Xu, H. Cheng, Z. Wang, C. Qi, J. Chen, S. Zhang, Synthesis of vertically standing MoS_2 triangles on SiC, Sci. Rep. 6 (2016) 31980.

[41] F. Giannazzo, S.E. Panasci, E. Schilirò, P. Fiorenza, G. Greco, F. Roccaforte, M. Cannas, S. Agnello, A. Koos, B. Pécz, M. Španková, Š. Chromik, Highly homogeneous 2D/3D heterojunction diodes by pulsed laser deposition of MoS_2 on ion implantation doped 4H-SiC, Adv. Mater. Interfac. 10 (2023) 2201502.

[42] K.V. Emtsev, A. Bostwick, K. Horn, J. Jobst, G.L. Kellogg, L. Ley, J.L. McChesney, T. Ohta, S.A. Reshanov, J. Rohrl, E. Rotenberg, A.K. Schmid, D. Waldmann, H. B. Weber, T. Seyller, Towards wafer-size graphene layers by atmospheric pressure graphitization of SiC(0001), Nat. Mater. 8 (2009) 203–207.

[43] C. Virojanadara, M. Syvajarvi, R. Yakimova, L.I. Johansson, A.A. Zakharov, T. Balasubramanian, Homogeneous large-area graphene layer growth on 6H-SiC (0001), Phys. Rev. B 78 (2008) 245403.

[44] M. Suemitsu, S. Jiao, H. Fukidome, Y. Tateno, I. Makabe, T. Nakabayashi, Epitaxial graphene formation on 3C-SiC/Si thin films, J. Phys. D Appl. Phys. 47 (2014) 094016.

[45] D.A. Katzmarek, Y. Yang, M.B. Ghasemian, K. Kalantar-Zadeh, R.W. Ziolkowski, F. Iacopi, Characteristics of epitaxial graphene on SiC/Si substrates in the radio frequency spectrum, IEEE Electron. Device Lett. 44 (2023) 297–300.

[46] F. La Via, M. Zimbone, C. Bongiorno, A. La Magna, G. Fisicaro, I. Deretzis, V. Scuderi, C. Calabretta, F. Giannazzo, M. Zielinski, R. Anzalone, M. Mauceri, D. Crippa, E. Scalise, A. Marzegalli, A. Sarikov, L. Miglio, V. Jokubavicius, M. Syväjärvi, R. Yakimova, P. Schuh, M. Schöler, M. Kollmuss, P. Wellmann, New approaches and understandings in the growth of cubic silicon carbide, Materials 14 (2021) 5348.

[47] F. Giannazzo, I. Deretzis, A. La Magna, F. Roccaforte, R. Yakimova, Electronic transport at monolayer-bilayer junctions in epitaxial graphene on SiC, Phys. Rev. B 86 (2012) 235422.

[48] K.V. Emtsev, F. Speck, T. Seyller, L. Ley, J.D. Riley, Interaction, growth, and ordering of epitaxial graphene on SiC{0001} surfaces: a comparative photoelectron spectroscopy study, Phys. Rev. B 77 (2008) 155303.

[49] F. Hiebel, P. Mallet, F. Varchon, L. Magaud, J.-Y. Veuillen, Graphene-substrate interaction on 6H-SiC(000-1): a scanning tunneling microscopy study, Phys. Rev. B 78 (2008) 153412.

[50] B. Jabakhanji, N. Camara, A. Caboni, C. Consejo, B. Jouault, P. Godignon, J. Camassel, Almost free standing graphene on SiC(000-1) and SiC(11-20), Mater. Sci. Forum 711 (2012) 235–241.

[51] M. Ostler, I. Deretzis, S. Mammadov, F. Giannazzo, G. Nicotra, C. Spinella, Th Seyller, A. La Magna, Direct growth of quasi-free-standing epitaxial graphene on nonpolar SiC surfaces, Phys. Rev. B 88 (2013) 085408.

[52] F. Giannazzo, I. Deretzis, G. Nicotra, G. Fisichella, C. Spinella, F. Roccaforte, A. La Magna, Electronic properties of epitaxial graphene residing on SiC facets probed by conductive atomic force microscopy, Appl. Surf. Sci. 291 (2014) 53–57.

[53] G. Nicotra, Q.M. Ramasse, I. Deretzis, A. La Magna, C. Spinella, F. Giannazzo, Delaminated graphene at silicon carbide facets: atomic scale imaging and spectroscopy, ACS Nano 7 (2013) 3045–3052.

[54] F. Giannazzo, I. Deretzis, G. Nicotra, G. Fisichella, Q.M. Ramasse, C. Spinella, F. Roccaforte, A. La Magna, High resolution study of structural and electronic properties of epitaxial graphene grown on off-axis 4H–SiC (0001), J. Cryst. Growth 393 (2014) 150–155.

[55] C. Bouhafs, A.A. Zakharov, I.G. Ivanov, F. Giannazzo, J. Eriksson, V. Stanishev, P. Kühne, T. Iakimov, T. Hofmann, M. Schubert, F. Roccaforte, R. Yakimova, V. Darakchieva, Multi-scale investigation of interface properties, stacking order and decoupling of few layer graphene on C-face 4H-SiC, Carbon 116 (2017) 722–732.

[56] G. Nicotra, I. Deretzis, M. Scuderi, C. Spinella, P. Longo, R. Yakimova, F. Giannazzo, A. La Magna, Interface disorder probed at the atomic scale for graphene grown on the C face of SiC, Phys. Rev. B 91 (2015) 155411.

[57] A. Michon, S. Vézian, A. Ouerghi, M. Zielinski, T. Chassagne, M. Portail, Direct growth of few-layer graphene on 6H-SiC and 3C-SiC/Si via propane chemical vapor deposition, Appl. Phys. Lett. 97 (2010) 171909.

[58] W. Strupinski, K. Grodecki, A. Wysmolek, R. Stepniewski, T. Szkopek, P. E. Gaskell, A. Grüneis, D. Haberer, R. Bozek, J. Krupka, J.M. Baranowski, Graphene epitaxy by chemical vapor deposition on SiC, Nano Lett. 11 (4) (2011) 1786–1791.

[59] A. Michon, S. Vézian, E. Roudon, D. Lefebvre, M. Zielinski, T. Chassagne, M. Portail, Effects of pressure, temperature, and hydrogen during graphene growth on SiC(0001) using propane-hydrogen chemical vapor deposition, J. Appl. Phys. 113 (2013) 203501.

[60] F. Varchon, R. Feng, J. Hass, X. Li, B. Ngoc Nguyen, C. Naud, P. Mallet, J.-Y. Veuillen, C. Berger, E.H. Conrad, L. Magaud, Electronic structure of epitaxial graphene layers on SiC: effect of the substrate, Phys. Rev. Lett. 99 (2007) 126805.

[61] F. Speck, J. Jobst, F. Fromm, M. Ostler, D. Waldmann, M. Hundhausen, H. B. Weber, Th Seyller, The quasi-free-standing nature of graphene on H-saturated SiC(0001), Appl. Phys. Lett. 99 (2011) 122106.

[62] N. Briggs, et al., Epitaxial graphene/silicon carbide intercalation: a mini-review on graphene modulation and unique 2D materials, Nanoscale 11 (2019) 15440.

[63] C. Riedl, C. Coletti, T. Iwasaki, A.A. Zakharov, U. Starke, Quasi-free-standing epitaxial graphene on SiC obtained by hydrogen intercalation, Phys. Rev. Lett. 103 (2009) 246804.

[64] K. Yamasue, H. Fukidome, K. Funakubo, M. Suemitsu, Y. Cho, Interfacial charge states in graphene on SiC studied by noncontact scanning nonlinear dielectric potentiometry, Phys. Rev. Lett. 114 (2015) 226103.

[65] S. Sonde, F. Giannazzo, V. Raineri, R. Yakimova, J.-R. Huntzinger, A. Tiberj, J. Camassel, Electrical properties of the graphene/4H-SiC (0001) interface probed by scanning current spectroscopy, Phys. Rev. B 80 (2009) 241406 (R).

[66] S. Hertel, D. Waldmann, J. Jobst, A. Albert, M. Albrecht, S. Reshanov, A. Schöner, M. Krieger, H.B. Weber, Tailoring the graphene/silicon carbide interface for monolithic wafer-scale electronics, Nat. Commun. 3 (2012) 957.

[67] F. Giannazzo, S. Hertel, A. Albert, G. Fisichella, A. La Magna, F. Roccaforte, M. Krieger, H.B. Weber, Electrical properties of the hydrogen intercalated epitaxial graphene/SiC interface investigated by nanoscale current mapping, Mater. Sci. Forum 821–823 (2015) 929.

[68] F. Giannazzo, I. Shtepliuk, I.G. Ivanov, T. Iakimov, A. Kakanakova-Georgieva, E. Schilirò, P. Fiorenza, R. Yakimova, Probing the uniformity of hydrogen intercalation in quasi-free-standing epitaxial graphene on SiC by micro-Raman mapping and conductive atomic force microscopy, Nanotechnology 30 (2019) 284003.

[69] S. Hertel, M. Krieger, H.B. Weber, Monolithic circuits with epitaxial graphene/silicon carbide transistors, Phys. Status Solidi RRL 8 (2014) 688–691.

[70] J. Zhao, P. Ji, Y. Li, R. Li, K. Zhang, H. Tian, K. Yu, B. Bian, L. Hao, X. Xiao, W. Griffin, N. Dudeck, R. Moro, L. Ma, W.A. de Heer, Ultrahigh-mobility semiconducting epitaxial graphene on silicon carbide, Nature 625 (2024) 60–65.

[71] Q.H. Wang, K.K. Zadeh, A. Kis, J.N. Coleman, M.S. Strano, Electronics and optoelectronics of two-dimensional transition metal dichalcogenides, Nat. Nanotechnol. 7 (2012) 699.

[72] B. Radisavljevic, A. Radenovic, J. Brivio, V. Giacometti, A. Kis, Single-layer MoS_2 transistors, Nat. Nanotechnol. 6 (2011) 147–150.

[73] S.E. Panasci, I. Deretzis, E. Schilirò, A. La Magna, F. Roccaforte, A. Koos, B. Pécz, S. Agnello, M. Cannas, F. Giannazzo, Interface structure and doping of CVD grown MoS_2 on 4H-SiC by microscopic analyses and ab initio calculations, Phys. Status Solidi RRL 17 (2023) 2300218.

[74] C.R. Serrao, A.M. Diamond, S.-L. Hsu, L. You, S. Gadgil, J. Clarkson, C. Carraro, R. Maboudian, C. Hu, S. Salahuddin, Highly crystalline MoS_2 thin films grown by pulsed laser deposition, Appl. Phys. Lett. 106 (2015) 052101.

[75] S.E. Panasci, A. Koos, E. Schilirò, S. Di Franco, G. Greco, P. Fiorenza, F. Roccaforte, S. Agnello, M. Cannas, F.M. Gelardi, A. Sulyok, M. Nemeth, B. Pécz, F. Giannazzo, Multiscale investigation of the structural, electrical and photoluminescence properties of MoS_2 obtained by MoO_3 sulfurization, Nanomaterials 12 (2022) 182.

[76] F. Giannazzo, S.E. Panasci, E. Schilirò, G. Greco, F. Roccaforte, G. Sfuncia, G. Nicotra, M. Cannas, S. Agnello, E. Frayssinet, Y. Cordier, A. Michon, A. Koos, B. Pécz, Atomic resolution interface structure and vertical current injection in highly uniform MoS_2 heterojunctions with bulk GaN, Appl. Surf. Sci. 631 (2023) 157513.

[77] M. Španková, Š. Chromik, E. Dobročka, L.P. Slušná, M. Talacko, M. Gregor, B. Pécz, A. Koos, G. Greco, S.E. Panasci, P. Fiorenza, F. Roccaforte, Y. Cordier, E. Frayssinet, F. Giannazzo, Large-area MoS_2 films grown on sapphire and GaN substrates by pulsed laser deposition, Nanomaterials 13 (2023) 2837.

[78] F. Roccaforte, P. Fiorenza, R. Lo Nigro, F. Giannazzo, G. Greco, Physics and technology of gallium nitride materials for power electronics, Riv. Nuovo Cimento 41 (2018) 625–680.

[79] J. Kim, C. Bayram, H. Park, C.-W. Cheng, C. Dimitrakopoulos, J.A. Ott, K. B. Reuter, S.W. Bedell, D.K. Sadana, Principle of direct van der Waals epitaxy of single-crystalline films on epitaxial graphene, Nat. Commun. 5 (2014) 4836.

[80] J.-H. Min, K.-H. Li, Y.-H. Kim, J.-W. Min, C.H. Kang, K.-H. Kim, J.-S. Lee, K.J. Lee, S.-M. Jeong, D.-S. Lee, S.-Y. Bae, T.K. Ng, B.S. Ooi, Toward large-scale Ga_2O_3 membranes via quasi-van der Waals epitaxy on epitaxial graphene layers, ACS Appl. Mater. Interfaces 13 (2021) 13410–13418.

[81] P. Gupta, A.A. Rahman, S. Subramanian, S. Gupta, A. Thamizhavel, T. Orlova, S. Rouvimov, S. Vishwanath, V. Protasenko, M.R. Laskar, H.G. Xing, D. Jena, A. Bhattacharya, Layered transition metal dichalcogenides: promising near lattice-matched substrates for GaN growth, Sci. Rep. 6 (2016) 23708.

[82] M. Tangi, P. Mishra, T.K. Ng, M.N. Hedhili, B. Janjua, M.S. Alias, D.H. Anjum, C.-C. Tseng, Y. Shi, H.J. Joyce, L.-J. Li, B.S. Ooi, Determination of band offsets at GaN/single-layer MoS_2 heterojunction, Appl. Phys. Lett. 109 (2016) 032104.

[83] Z.Y. Al Balushi, K. Wang, R.K. Ghosh, R.A. Vilá, S.M. Eichfeld, J.D. Caldwell, X. Qin, Y.-C. Lin, P.A. De Sario, G. Stone, S. Subramanian, D.F. Paul, R. M. Wallace, S. Datta, J.M. Redwing, J.A. Robinson, Two-dimensional gallium nitride realized via graphene encapsulation, Nat. Mater. 15 (2016) 1166.

[84] G. Sfuncia, G. Nicotra, F. Giannazzo, B. Pécz, G.K. Gueorguiev, A. Kakanakova-Georgieva, 2D graphitic-like gallium nitride and other structural selectivity in confinement at the graphene/SiC interface, CrystEngComm 25 (2023) 5810–5817.

[85] B. Pécz, G. Nicotra, F. Giannazzo, R. Yakimova, A. Koos, A. Kakanakova-Georgieva, Indium nitride at the 2D limit, Adv. Mater. 33 (2021) 2006660.

[86] A. Kakanakova-Georgieva, G.K. Gueorguiev, D.G. Sangiovanni, N. Suwannaharn, I.G. Ivanov, I. Cora, B. Pécz, G. Nicotra, F. Giannazzo, Nanoscale phenomena ruling deposition and intercalation of AlN at the graphene/SiC interface, Nanoscale 12 (2020) 19470.

[87] A. Kakanakova-Georgieva, I.G. Ivanov, N. Suwannaharn, C.-W. Hsu, I. Cora, B. Pécz, F. Giannazzo, D.G. Sangiovanni, G.K. Gueorguiev, MOCVD of AlN on epitaxial graphene at extreme temperatures, CrystEngComm 23 (2021) 385–390.

[88] A. Kakanakova-Georgieva, F. Giannazzo, G. Nicotra, I. Cora, G.K. Gueorguiev, P. O.Å. Persson, B. Pécz, Material proposal for 2D indium oxide, Appl. Surf. Sci. 548 (2021) 149275.

[89] F. Turker, C. Dong, M.T. Wetherington, H. El-Sherif, S. Holoviak, Z.J. Trdinich, E. T. Lawson, G. Krishnan, C. Whittier, S.B. Sinnott, N. Bassim, J.A. Robinson, 2D oxides realized via confinement heteroepitaxy, Adv. Funct. Mater. 33 (2022) 2210404.

[90] B. Pécz, M. Nemeth, F. Giannazzo, A. Kakanakova-Georgieva, On the possibility of realizing a 2D structure of Si-N bonds by metal-organic chemical vapor deposition, Phys. Status Solidi B 260 (2023) 2300262.

[91] C.M. Polley, H. Fedderwitz, T. Balasubramanian, A.A. Zakharov, R. Yakimova, O. Bäcke, J. Ekman, S.P. Dash, S. Kubatkin, S. Lara-Avila, Bottom-up growth of monolayer honeycomb SiC, Phys. Rev. Lett. 130 (2023) 076203.

[92] Y.-M. Lin, D.B. Farmer, K.A. Jenkins, Y. Wu, J.L. Tedesco, R.L. Myers-Ward, C. R. Eddy Jr., D. Kurt Gaskill, C. Dimitrakopoulos, P. Avouris, Enhanced performance in epitaxial graphene FETs with optimized channel morphology, IEEE Electron. Device Lett. 32 (2011) 1343.

[93] Z. Guo, R. Dong, P.S. Chakraborty, N. Lourenco, J. Palmer, Y. Hu, M. Ruan, J. Hankinson, J. Kunc, J.D. Cressler, C. Berger, W.A. de Heer, Record maximum oscillation frequency in C-face epitaxial graphene transistors, Nano Lett. 13 (2013) 942–947.

[94] C. Yu, Z.Z. He, X.B. Song, Q.B. Liu, T.T. Han, S.B. Dun, J.J. Wang, C.J. Zhou, J. C. Guo, Y.J. Lv, Z.H. Feng, S.J. Cai, Improvement of the frequency characteristics of graphene field-effect transistors on SiC substrate, IEEE Electron. Device Lett. 38 (2017) 1339–1342.

[95] Z. He, C. Yu, Q. Liu, X. Song, X. Gao, J. Guo, C. Zhou, S. Cai, Z. Feng, High temperature RF performances of epitaxial bilayer graphene field effect transistors on SiC substrates, Carbon 164 (2020) 435–441.

[96] Y.-M. Lin, A. Valdes-Garcia, S.-J. Han, D.B. Farmer, I. Meric, Y. Sun, Y. Wu, C. Dimitrakopoulos, A. Grill, P. Avouris, K.A. Jenkins, Wafer-scale graphene integrated circuit, Science 332 (2011) 1294.

[97] O. Habibpour, Z. Simon He, W. Strupinski, N. Rorsman, H. Zirath, Wafer scale millimeter-wave integrated circuits based on epitaxial graphene in high data rate communication, Sci. Rep. 7 (2017) 41828.

[98] E. Schilirò, R. Lo Nigro, F. Roccaforte, F. Giannazzo, Recent advances in seeded and seed-layer-free atomic layer deposition of high-K dielectrics on graphene for electronics, C – Journal of Carbon Research 5 (2019) 53.

[99] B. Dlubak, P.R. Kidambi, R.S. Weatherup, S. Hofmann, J. Robertson, Substrate-assisted nucleation of ultra-thin dielectric layers on graphene by atomic layer deposition, Appl. Phys. Lett. 100 (2012) 173113.

[100] E. Schilirò, R. Lo Nigro, S.E. Panasci, S. Agnello, M. Cannas, F.M. Gelardi, F. Roccaforte, F. Giannazzo, Direct atomic layer deposition of ultrathin aluminum oxide on monolayer MoS_2 exfoliated on gold: the role of the substrate, Adv. Mater. Interfac. 6 (2019) 1900097.

[101] E. Schilirò, S.E. Panasci, A.M. Mio, G. Nicotra, S. Agnello, B. Pecz, G.Z. Radnoczi, I. Deretzis, A. La Magna, F. Roccaforte, R. Lo Nigro, F. Giannazzo, Direct atomic layer deposition of ultra-thin Al_2O_3 and HfO_2 films on gold-supported monolayer MoS_2, Appl. Surf. Sci. 630 (2023) 157476.

[102] E. Schilirò, R. Lo Nigro, F. Roccaforte, I. Deretzis, A. La Magna, A. Armano, S. Agnello, B. Pecz, I.G. Ivanov, R. Yakimova, F. Giannazzo, Seed-layer-free atomic layer deposition of highly uniform Al_2O_3 thin films onto monolayer epitaxial graphene on silicon carbide, Adv. Mater. Interfac. (2019) 1–11, 1900097.

[103] E. Schilirò, R. Lo Nigro, S.E. Panasci, F.M. Gelardi, S. Agnello, R. Yakimova, F. Roccaforte, F. Giannazzo, Aluminum oxide nucleation in the early stages of atomic layer deposition on epitaxial graphene, Carbon 169 (2020) 172–181.

[104] F. Bianco, D. Perenzoni, D. Convertino, S.L. De Bonis, D. Spirito, M. Perenzoni, C. Coletti, M.S. Vitiello, A. Tredicucci, Terahertz detection by epitaxial-graphene field-effect-transistors on silicon carbide, Appl. Phys. Lett. 107 (2015) 131104.

[105] H. Qin, J. Sun, S. Liang, X. Li, X. Yang, Z. He, C. Yu, Z. Feng, Room-temperature, low-impedance and high-sensitivity terahertz direct detector based on bilayer graphene field-effect transistor, Carbon 116 (2017) 760–765.

[106] C. Sorger, S. Preu, J. Schmidt, S. Winnerl, Y.V. Bludov, N.M.R. Peres, M. I. Vasilevskiy, H. B Weber, Terahertz response of patterned epitaxial graphene, New J. Phys. 17 (2015) 053045.

[107] X. Cai, A.B. Sushkov, M.M. Jadidi, L.O. Nyakiti, R.L. Myers-Ward, D.K. Gaskill, T. E. Murphy, M.S. Fuhrer, H.D. Drew, Plasmon-enhanced terahertz photodetection in graphene, Nano Lett. 15 (2015) 4295–4302.

[108] A. El Fatimy, A. Nath, B.D. Kong, A.K. Boyd, R.L. Myers-Ward, K.M. Daniels, M. M. Jadidi, T.E. Murphy, D.K. Gaskill, P. Barbara, Ultra-broadband photodetectors based on epitaxial graphene quantum dots, Nanophotonics 7 (2018) 735–740.

[109] M.T. Schlecht, S. Preu, S. Malzer, H.B. Weber, An efficient Terahertz rectifier on the graphene/SiC materials platform, Sci. Rep. 9 (2019) 11205.

[110] Y. Xu, D. Zhou, H. Lu, D. Chen, F. Ren, R. Zhang, Y. Zheng, High-temperature and reliability performance of 4H-SiC Schottky-barrier photodiodes for UV detection, J. Vac. Sci. Technol. B 33 (2015) 040602.

[111] W.-C. Lien, D.-S. Tsai, D.-H. Lien, D.G. Senesky, H. He, A.P. Pisano, 4H-SiC metal-semiconductor-metal ultraviolet photodetectors in operation of 450 °C, IEEE Electron. Device Lett. 33 (2012) 1586.

[112] A. Sciuto, F. Roccaforte, S. Di Franco, V. Raineri, G. Bonanno, High responsivity Schottky UV photodiodes based on the pinch-off surface effect, Appl. Phys. Lett. 89 (2006) 081111.

[113] Y.-K. Su, Y.-Z. Chiou, C.-S. Chang, S.-J. Chang, Y.-C. Lin, J.F. Chen, 4H-SiC metal-semiconductor-metal ultraviolet photodetectors with Ni/ITO electrodes, Solid State Electron. 46 (2002) 2237.

[114] M. Badila, G. Brezeanu, J. Millan, P. Godignon, M.L. Locatelli, J.P. Chante, A. Lebedev, P. Lungu, G. Dinca, V. Banu, G. Banoiu, Diam. Relat. Mater. 9 (2000) 994.

[115] X. Li, R. Wang, Z. Zuo, L. Ge, X. Chen, X. Xie, L. Xiao, Y. Peng, X. Xu, X. Hu, Correlation between the response performance of epitaxial graphene/SiC UV-photodetectors and the number of carriers in graphene, Carbon 183 (2021) 590–599.

[116] Y. Li, P. Chen, X. Chen, R. Xu, M. Liu, J. Zhou, C. Ge, H. Peng, X. Mao, J. Feng, X. Hu, Y. Peng, X. Xu, Z. Xie, X. Xiu, D. Chen, B. Liu, P. Han, Y. Shi, R. Zhang, Y. Zheng, High-responsivity graphene/4H-SiC ultraviolet photodetector based on a planar junction formed by the dual modulation of electric and light fields, Adv. Opt. Mater. 8 (2020) 2000559.

[117] J. Yang, L. Guo, Y. Guo, W. Hu, Z. Zhang, Epitaxial graphene/SiC Schottky ultraviolet photodiode with orders of magnitude adjustability in responsivity and response speed, Appl. Phys. Lett. 112 (2018) 103501.

[118] T.J. Anderson, K.D. Hobart, J.D. Greenlee, D.I. Shahin, A.D. Koehler, M.J. Tadjer, E.A. Imhoff, R.L. Myers-Ward, A. Christou, F.J. Kub, Ultraviolet detector based on graphene/SiC heterojunction, APEX 8 (2015) 041301.

[119] K. Zhang, M. Peng, A. Yu, Y. Fan, J. Zhai, Z.L. Wang, A substrate-enhanced MoS_2 photodetector through a dual-photogating effect, Mater. Horiz. 6 (2019) 826.